T H E U N I V E R S I T Y O F M I C H I G A N
COLLEGE OF ENGINEERING
Department of Meteorology and Oceanography

MEASUREMENT AND ANALYSIS OF THE STRUCTURE OF TURBULENCE NEAR THE GROUND WITH A HOT WIRE ANEMOMETER SYSTEM

W. Gale Biggs

Donald J. Portman, Project Director

sponsored by:

COLD REGIONS RESEARCH LABORATORY
GRANT NO. DOD-DA-AMC-27-021-63-G7
and
NATIONAL SCIENCE FOUNDATION
GRANT NO. G-22388

administered through:

OFFICE OF RESEARCH ADMINISTRATION ANN ARBOR

June 1966

engn
UMR 1355

This report was also a dissertation submitted in partial fulfillment of the requirements for the degree of Doctor of Philosophy in The University of Michigan, 1966.

ABSTRACT

Spectral measurements of atmospheric turbulence near the ground have demonstrated for the periods examined the presence of a buoyant subrange at high frequencies. The existence of the buoyant subrange effectively precludes the establishment of local isotropy.

This result has been achieved in a field study using recently developed equipment employing the constant temperature hot wire anemometer. The output of the constant temperature hot wire anemometer, as contrasted with that of the constant current mode, is independent of changes in the mean wind speed and can, therefore, be linearized. The response characteristics of the hot wire permit the extension of the range of measurements into the high frequency fluctuations of the turbulent field.

In the present investigation, the configuration of hot wires was such that all three components of the wind were obtained. The spectral densities were computed for each wind component. These quantities were then analyzed to ascertain the degree to which they conform with Kolmogoroff's theory of local isotropy. The analysis shows the existence of a buoyant subrange at frequencies that are beyond the sensing capability of most meteorological instruments. The measurements were made at 1 m above the earth's surface in lapse conditions; local isotropy was not found in spite of the fact that excellent agreement with the -5/3 power law is shown relating the spectrum and the frequency.

ACKNOWLEDGMENTS

The author wishes to thank all who assisted him during the progress of this study. The advice and guidance of Professor Donald J. Portman, Chairman of the Doctoral Committee, is particularly appreciated. The author is also grateful to Professors Walter R. Debler, E. Wendell Hewson, and Aksel Wiin-Nielsen for serving as members of the Committee and for their willingness to help.

Especial thanks are due Fred V. Brock who provided vital technical and computing assistance throughout the undertaking.

In addition, Edward Ryznar, Floyd Elder, and Arifhusen Waqif assisted in various phases with both technical and moral support.

The author is grateful for financial support received from the Cold Regions Research Laboratories under Grant No. DOD-DA-AMC-27-021-63-G7 and to the National Science Foundation under Grant NSF-G-22388. In addition, some support was received from the Weather Bureau under contracts Cwb-10964 and Cwb-10714. The author also wishes to acknowledge the support of the University of Michigan through the use of the IBM 7090 at the Computing Center, Professor R. C. F. Bartels, Director.

TABLE OF CONTENTS

		Page
List of Tables		v
List of Figures		vi
	Chapter I	
	General Introduction and Concepts	
1.1	Introduction	1
1.2	Atmospheric Turbulence	2
1.3	Local Isotropy	9
	Chapter II	
	Description of Equipment and Experiment	
2.1	Introduction	13
2.2	Hot Wire Anemometers	13
	2.2.1 Model M-5 Hot Wire Amplifier Unit	25
	2.2.2 Hot Wire Probes	28
2.3	Calibration of the Hot Wire Anemometers	30
2.4	Error Analysis for Data Collection	39
2.5	Field Measurements	46
	Chapter III	
	Data Reduction and Processing	
3.1	Introduction	58
3.2	The Equations Used	60
3.3	The Computer Processing	65
	Chapter IV	
	Results and Conclusions	
4.1	Introduction	72
4.2	Data Selection and Results	73
	4.2.1 29 April 65	74

TABLE OF CONTENTS (concluded)

	Page
4.2.1.1 Gradient Relationships for the Period of 1430-1442 (4/29/65)	75
4.2.1.2 Turbulent Characteristics for the Period of 1430-1442 (4/29/65)	78
4.2.2 21 January 65	89
4.2.2.1 Gradient Relationships for the Period of 1220-1232 (1/21/65)	92
4.2.2.2 Turbulent Characteristics for the Period of 1220-1232 (1/21/65)	92
4.2.2.3 Gradient Relationships for the Period of 1300-1312 (1/21/65)	97
4.2.2.4 Turbulent Characteristics for the Period of 1300-1312 (1/21/65)	97
4.2.2.5 Gradient Relationships for the Period of 1308-1320 (1/21/65)	102
4.2.2.6 Turbulent Characteristics for the Period of 1308-1320 (1/21/65)	102
4.3 Comparison of Turbulence and Gradient Relationships	105
4.4 Summary	111
Appendix	114
Bibliography	121

LIST OF TABLES

		Page
Tables		
2-1	Summary of advantages and disadvantages associated with the constant current and constant resistance modes of hot wire operation.	24
2-2	Coefficients for the hot wire equation 2-13 and other constants used in equation 2-11.	36
2-3	Percent error in wind speed given as a function of temperature fluctuation and wind speed.	42
4-1	Gradient and turbulence parameters for the selected intervals.	108

LIST OF FIGURES

Figures		Page
1-1	Diagram illustrating the correlation functions f(r) and g(r).	6
2-1	The uncompensated constant current hot wire anemometer.	16
2-2	The compensated constant current hot wire anemometer.	17
2-3	The constant resistance (temperature) hot wire anemometer.	18
2-4	The constant resistance ratio hot wire anemometer.	19
2-5	The model M-5 hot wire amplifier unit.	26
2-6	The wiring diagram for the model M-5 hot wire amplifier unit.	26
2-7	Diagram illustrating wind components as sensed by the X-probe.	30
2-8	A plot of U_o vs T where U_o is in ft/sec and T in ^oF.	38
2-9	Noise level spectrum for 7-channel tape recorder and wave analyzer.	44
2-10	Aerial view looking west into Willow Run Airport showing location of instrument array.	47
2-11	Top view of Willow Run Airport.	48
2-12	View of test site and truck used to house the electronics.	49
2-13	Three meter portable tower for mounting hot wire probes and temperature sensors.	51
2-14	Close-up of hot wire probes, temperature sensor, and mounting bracket.	52
2-15	Close-up of the sampling space showing the configuration of the four hot wires and the temperature sensor.	54

LIST OF FIGURES (continued)

Figures		Page
2-16	The carrying case lined with foam padding for transporting the hot wire probes.	55
2-17	The four hot wire amplifiers mounted on the chassis showing the necessary control switches.	56
3-1	Hybrid computer system in the Department of Meteorology and Oceanography (Described in the Appendix).	59
3-2	The horizontal wind components as measured relative to the hot wires.	60
3-3	The vertical wind component as measured relative to the hot wires.	61
3-4	Schematic diagram showing the computer processing.	65
3-5	Computation of $\overline{f(t)}$ in accordance with equation 3-15.	67
3-6	Analog tape loop recorder/reproducer, wave analyzer, and 7-channel tape recorder/reproducer.	71
4-1	Wind and temperature profiles for period 1430-1442 (4/29/65).	76
4-2	Spectral densities for u, v, w for period 1430-1442 (4/29/65) calculated for a bandwidth of 0.3 cps.	79
4-3	Frequency times energy plotted vs reduced frequency for u, v, w for period 1430-1442 (4/29/65) calculated for a bandwidth of 0.3 cps.	81
4-4	Schematic representation of the various spectral regions as a function of height based on the results of others and the analysis as presented in this study.	90

LIST OF FIGURES (concluded)

Figures		Page
4-5	Wind and temperature profiles for period 1220-1232 (1/21/65).	93
4-6	Spectral densities for u, v, w for period 1220-1232 (1/21/65) calculated for a bandwidth of 0.3 cps.	94
4-7	Frequency times energy plotted vs reduced frequency for u, v, w for period 1220-1232 (1/21/65) calculated for a bandwidth of 0.3 cps.	96
4-8	Wind and temperature profiles for period 1300-1312 (1/21/65).	98
4-9	Spectral densities for u, v, w for period 1300-1312 (1/21/65) calculated for a bandwidth of 0.3 cps.	100
4-10	Frequency times energy plotted vs reduced frequency for u, v, w for period 1300-1312 (1/21/65) calculated for a bandwidth of 0.3 cps.	101
4-11	Wind and temperature profiles for period 1308-1320 (1/21/65).	103
4-12	Spectral densities for u, v, w for period 1308-1320 (1/21/65) calculated for a bandwidth of 0.3 cps.	104
4-13	Frequency times energy plotted vs reduced frequency of u, v, w for period 1308-1320 (1/21/65) calculated for a bandwidth of 0.3 cps.	106

Chapter I

General Introduction and Concepts

1.1 Introduction

Experimental investigations of turbulence near the ground have, in the past, been confined generally to measuring the average flow properties. Only recently has technology advanced to the point where a more direct measurement of the structure of atmospheric turbulence could be made. With the development of relatively stable electronic equipment for constant temperature hot wire anemometers, a breakthrough was possible. The stability of the electronic circuits has been greatly improved because of recent advances in transistors which allow the impedance of hot wire and amplifier to be more easily matched. The advantage of the constant temperature method over the constant current mode is that the output is representative of the flow field at any wind speed; the constant current mode is representative only at a preset value of the wind speed. Another advantage of the hot wire technique is the fast response of the sensing element which extends the range of measurements well beyond the previous capacity of meteorological instrumentation.

The development of the constant temperature mode of operation has allowed the effective use of the hot wire in the study of atmospheric turbulence. Important characteristics of the flow field are the spectral densities of the three components of the wind. From these properties it is possible, for example, to determine the degree of local isotropy and the scales within which isotropic considerations are valid. When isotropy exists the spectral densities of the v and w components must be equal and greater than the spectral density of the u component of the wind. These relationships are discussed in the next two sections and the measured quantities are compared with the expected results in Chapter IV.

The present study is important because the only significant application of general turbulence theory to the atmosphere is in the region wherein isotropy can be shown.

1.2 Atmospheric Turbulence

A flow with a fluctuating characteristic is conveniently thought of as consisting of two components, one of which is a mean flow that is steady, and the other a fluctuating flow whose time-averaged velocity is everywhere zero. Atmospheric

fluctuations can range in scale from thousands of kilometers to millimeters. Thus, when speaking of atmospheric turbulence, one should take care to define within which scale the problem is formulated.

To discuss the concepts postulated about turbulent fields, however, a more precise definition of turbulence is required. Thus far, turbulence has been conceived as a time-varying flow. It is not sufficient to define turbulence as irregular in time alone. Hinze (1959) defines turbulence as follows: "Turbulent fluid motion is an irregular condition of flow in which the various quantities show a random variation with time and space coordinates, so that statistically distinct average values can be discerned."

In the very beginning of turbulence investigations, Reynolds (1894) showed that as a consequence of turbulence in a flowing fluid there are apparent shearing stresses that are essential in determining the behavior of the mean flow. The interrelationship between the Reynolds stresses and the mean flow is the most important aspect of turbulence problems, and considerable attention is directed to it. There resulted a number of theories, such as the similarity theory of von Karmen (1924) and the mixing-length theories, in particular the momentum-transfer theory of Prandtl (1925, 1927) and the

vorticity-transfer theory of Taylor (1932). These theories, however, while permitting the prediction of certain gross characteristics of some boundary layer turbulent flows, offered only limited understanding of the mechanism of turbulence.

Starting in 1935 G. I. Taylor gave impetus and new direction to turbulent research through the introduction and application of certain statistical concepts to turbulence problems. Some of the concepts that led to the definition of certain quantities important in the characterization of turbulent fields are:

(1) The spectrum of turbulence which may be used to describe the time variation of velocity at any point in the flow field as an infinite sum of harmonic components (a Fourier integral) each of which has a different and characteristic scale (or eddy size) associated with it. Alternatively, the turbulent field at any instant of time may be thought of as defined in space by a three-dimensional Fourier integral.

(2) The correlation of velocities in a turbulent field which in atmospheric turbulence generally decrease as the distance between neighboring points increases.

(3) The condition of isotropy is a particularly important characteristic of turbulent fields. It involves the degree to which the quantitative description of the field at a certain point depends upon the orientation of the physical coordinate system.

The basic definition of turbulence is in terms of the complete joint-probability function for the velocity components at all points in space. Clearly, in practice, the measurement and calculation of the moment generating function describing the statistical behavior is impossible. Because of the comparative simplicity and convenience of the correlation and spectrum functions, they play a central role in current theoretical and experimental work. Great care, however, should be exercised in using the correlation and spectrum functions as complete descriptions of the turbulent motion. A central point discussed in this thesis (Chapter IV) is the inference about local isotropy deduced on the basis of a spectrum that displays the -5/3 law.

Correlation functions of interest are defined by

$$f(r) = \frac{\overline{u'_1 u'_2}}{\overline{u'^2}} \qquad 1\text{-}1$$

and

$$g(r) = \frac{\overline{v_1' v_2'}}{\overline{v'^2}} \qquad 1\text{-}2$$

where $u = \bar{u} + u'$ and $v = \bar{v} + v'$ are the instantaneous components of the velocity in the x and y direction. The overbar denotes the time mean. The subscript 2 represents a velocity at some distance r away from u_1. Figure 1-1 illustrates the components for the two correlation functions f(r) and g(r) in isotropic turbulence.

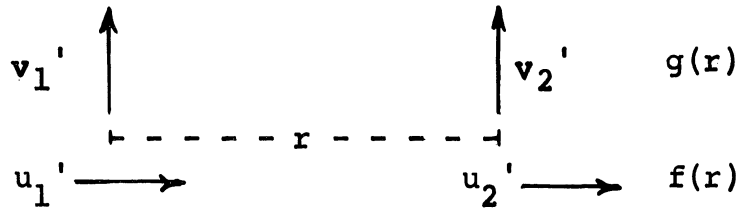

Figure 1-1. Diagram illustrating the correlation functions f(r) and g(r).

It is convenient to designate f(r) a longitudinal correlation coefficient and g(r) a transverse correlation coefficient.

Several concepts can now be defined in terms of the f(r) and g(r) functions. If the mean velocity field is independent of time and if f(r) is a symmetrical (or even) function of r (i.e., f(r) = f(-r)), then the field is called stationary.

For a three-dimensional velocity field the concept of stationarity generalizes to the concept of homogeneity. Thus if the mean value of the vector velocity is constant

and if both f(r) and g(r) are even functions of r, then the vector field is called homogeneous. A homogeneous field is called isotropic if it is unaffected by a rotation or reflection of the axes of reference. The quantities $\overline{u'^2}$, $\overline{v'^2}$ and $\overline{w'^2}$ are then all equal as well as uniform in space.

Von Karman and Howarth (1937) established a relation between f(r) and g(r) for the special case of isotropic turbulence

$$f(r) - g(r) = -\frac{r}{2}\frac{\partial f(r)}{\partial r} \qquad 1\text{-}3$$

Using measurements of Simmons and Salter, Taylor (1938) experimentally verified equation 1-3. He showed further that the correlation function is the Fourier transform of the frequency spectrum F(f). Thus

$$f(r) = \int_0^\infty F_{f(r)}(f) \cos \frac{2\pi f r}{\bar{U}}\, df \qquad 1\text{-}4$$

and conversely

$$F_{f(r)}(f) = \frac{4}{\bar{U}} \int_0^\infty f(r) \cos \frac{2\pi f r}{\bar{U}}\, dr \qquad 1\text{-}5$$

For g(r) the corresponding relationships are

$$g(r) = \int_0^\infty F_{g(r)}(f) \cos \frac{2\pi f r}{\bar{U}}\, df \qquad 1\text{-}6$$

and

$$F_{g(r)}(f) = \frac{4}{\bar{U}} \int_0^\infty g(r) \cos \frac{2\pi f r}{\bar{U}}\, dr \qquad 1\text{-}7$$

Application of equation 1-5 and 1-7 to equation 1-3 gives the corresponding relationship between the longitudinal spectrum $F_{f(r)}$ and the transverse spectrum $F_{g(r)}$.

$$F_{g(r)}(f) = \frac{1}{2} F_{f(r)}(f) - \frac{f}{2} \frac{dF_{f(r)}(f)}{df} \qquad 1\text{-}8$$

Taylor (1938) made the assumption that for a stationary field

$$\frac{\partial}{\partial t} = - \bar{u} \frac{\partial}{\partial x}. \qquad 1\text{-}9$$

Equation 1-9 allows time series measurements to be used interchangeably with space measurements.

Hinze (1959) shows that equation 1-9 holds approximately only if u' is small with respect to $\bar{u}$. This can be shown by using the equation of motion,

$$\frac{\partial u}{\partial t} + u \frac{\partial u}{\partial x} = - \frac{1}{\rho} \frac{\partial p}{\partial x} + \nu \frac{\partial^2 u}{\partial x^2} \qquad 1\text{-}10$$

letting $u = \bar{u} + u'$ and since $\frac{\partial \bar{u}}{\partial t} = \frac{\partial \bar{u}}{\partial x} = 0$

$$\frac{\partial u'}{\partial t} + \bar{u} \frac{\partial u'}{\partial x} = - u' \frac{\partial u'}{\partial x} - \frac{1}{\rho} \frac{\partial p}{\partial x} + \nu \frac{\partial^2 u'}{\partial x^2} \qquad 1\text{-}11$$

The left-hand side of equation 1-11 corresponds to equation 1-9, and for Taylor's assumption to be useful, the sum of the terms on the right hand side of equation 1-11 must be very close to zero. The third term is small compared to the first two terms so a criterion would have to be such that it makes the first two terms small. One

criterion would be if $u'/\bar{u} \ll 1$ since this makes the pressure gradient term small also (p is of the order of ρu^2).

Uberoi and Corrsin (1953), Lin (1935), Ogura (1953) and Gifford (1956) have attempted theoretical evaluations of equation 1-9 in order to assess the error associated with its use. For the atmospheric case involving shear flow, even less can be said about the validity of equation 1-9. The velocity measurements by the hot wire anemometers are all time series measurements so Taylor's assumption must be accepted in order to use the theories of turbulence.

1.3 Local Isotropy

A major contribution toward the application of statistical methods to the study of turbulence was made by A. N. Kolmogoroff (1941) when he introduced the idea of local isotropy. Kolmogoroff postulated that for turbulence generated at large Reynolds numbers the small-scale components of the turbulence are approximately in statistical equilibrium. These small-scale components owe their existence to the non-linear interchange of energy between different wave number components. Kolmogoroff further postulated that the equilibrium would be dependent on only the viscosity of the

fluid (ν) and the energy dissipation per unit mass (ϵ).

The frequency bandwidth within which the above considerations apply is called the equilibrium range. It is a conservative system in that energy cascades from large to small eddies and that there is no external agency supplying energy in this region. If this bandwidth is of such an extent that the properties of the larger eddies are independent of the process by which the energy is converted to heat, then the region which depends primarily on the dissipation of energy by inertia forces is called the inertial subrange. In the inertial subrange the difference in the velocities at two points depends only on r and ϵ for small separations. For dimensional homogeneity

$$\overline{(u_2' - u_1')^2} \propto (\epsilon r)^{2/3}. \qquad 1\text{-}12$$

Expanding gives

$$1 - f(r) \propto (\epsilon r)^{2/3} \qquad 1\text{-}13$$

since $\overline{u_1'^2} = \overline{u_2'^2}$ = constant. From equation 1-5 the one-dimensional frequency spectrum is

$$F(f) \propto \epsilon^{2/3} f^{-5/3}. \qquad 1\text{-}14$$

Equation 1-14 is commonly referred to as the -5/3 law.

By assuming a form of the longitudinal spectrum as follows

$$F_f = Af^B \qquad 1\text{-}15$$

where A and B are constants, we can examine the relationships between the longitudinal and transverse components.

Using equation 1-15 in equation 1-8 and since

$$\frac{dF_f}{df} = AB\, f^{B-1} \qquad 1\text{-}16$$

we get

$$F_g = \frac{F_f}{2} - \frac{ABf}{2} f^{B-1} = F_f\left(\frac{1}{2} - \frac{B}{2}\right) \qquad 1\text{-}17$$

From equation 1-14 B = -5/3 so

$$F_g = 4/3\ F_f \qquad 1\text{-}18$$

Equation 1-18 shows that the transverse spectral density is <u>greater</u> than the longitudinal spectral density.

MacCready (1962) summarized data from the literature in order to set spectral limits on the inertial subrange. He states that the wave length of the lower limit is of the order of millimeters or centimeters in the troposphere and the upper limit in the neighborhood of 400 m for a height above the surface greater than 200 m. Shur (1962) and Reiter and Burns (1966) found the upper limit to be 600 m with their measurements taken at a height of from 9 to 11 km. Below 200 m, MacCready (1962) states that the upper limit is given by twice the height above the ground. For the data presented herein the upper limit would be expected to be 2 m since the data were taken at 1 m above the surface.

Chapter IV presents spectra measured by the hot wire anemometers and compares them with the expected results described above.

Chapter II

Description of Equipment and Experiment

2.1 Introduction

Before the results and subsequent conclusions can be evaluated or an assessment of the accuracy of the data collected can be made, an understanding of the method of data collection and analysis is necessary. Since both data collection and data processing are rather complex, a separate chapter is devoted to each. The present chapter discusses the instrumentation and the data collection techniques, while Chapter III describes the data processing methods. The last chapter presents the data in reduced form and gives the results and conclusions of this study.

The measuring system used was built for this study and is unique in meteorological investigations, so it is described in detail. Included in this chapter is a description pointing out the capabilities and limitations of the equipment, its field use, and the degree of reliability that can be assigned to the results.

2.2 Hot Wire Anemometers

The theoretical development of the flow around a hot wire whose length is large compared to its diameter has

been described by King (1914). The hot wire anemometer is heated by electrical means giving two typical cases for operation depending on whether the resistance or the current is maintained constant. In one case, the current heating the wire is kept constant, resulting in a wire temperature fluctuation according to the cooling effect of the ambient flow. In the other case, the current is controlled in such a manner that an appropriate amount of heat is being generated to maintain a constant temperature. In practical application the wire is in an intermediate state in which both its temperature and its heating current vary slightly, although it is desirable to keep one of the variations so small that it can be taken into account only as a correction. The quantity measured may be the resistance value itself, the heating current that is required to maintain a constant resistance, or the voltage drop across the wire. In the latter case both resistance and heating current may fluctuate. A complete description of the basic theory and operation of hot wire anemometers is given by Hinze (1959, Chapter 2).

The two modes of operation can be broken into four basic types of hot wire circuits, the "uncompensated

constant current" (figure 2-1), the "compensated constant current" (figure 2-2), the "constant resistance" (figure 2-3), and the "constant resistance ratio" (figure 2-4). The most common use is to place the hot wire in one arm of a Wheatstone Bridge circuit. All four types operate on the principle that the electrical resistance of a hot wire increases with its own absolute temperature so that the cooling produces a bridge unbalance. Each circuit has certain advantages in different applications, according to the bandwidth and response desired and is indicated in each figure.

The "constant current" mode (both compensated and uncompensated) is sensitive to variations of both the mean air velocity and mean temperature. Thus if either the mean wind or the mean temperature changes to a new mean value, the electronic components need to be readjusted.

The "constant temperature" mode is independent of changes in the mean wind and therefore does not need readjustment if the mean wind shifts. In addition the "constant resistance ratio" is independent of changes in either the mean wind or mean temperature. The "constant resistance ratio" circuit is such that the ratio of the resistance of the hot wire to an identical but unheated wire is

UNCOMPENSATED CONSTANT CURRENT

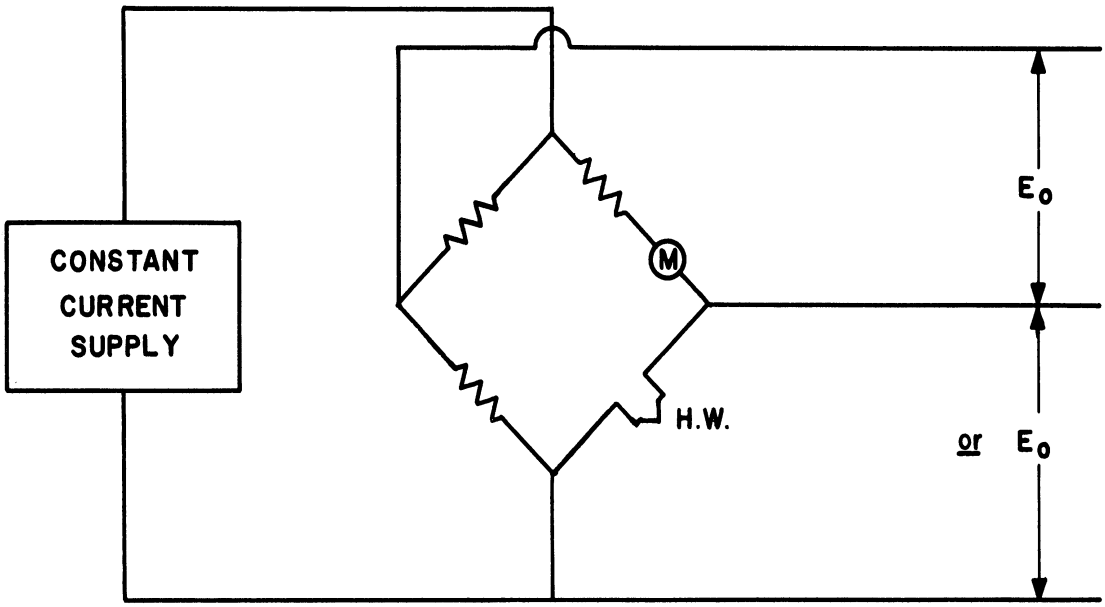

TYPICAL BAND : D.C. TO 100 cps

TYPICAL NOISE LEVEL (% OF AVE. VEL.) : 0.001 %

Figure 2-1. The uncompensated constant current hot wire anemometer. The hot wire is shown as one arm of the Wheatstone Bridge.

COMPENSATED CONSTANT CURRENT

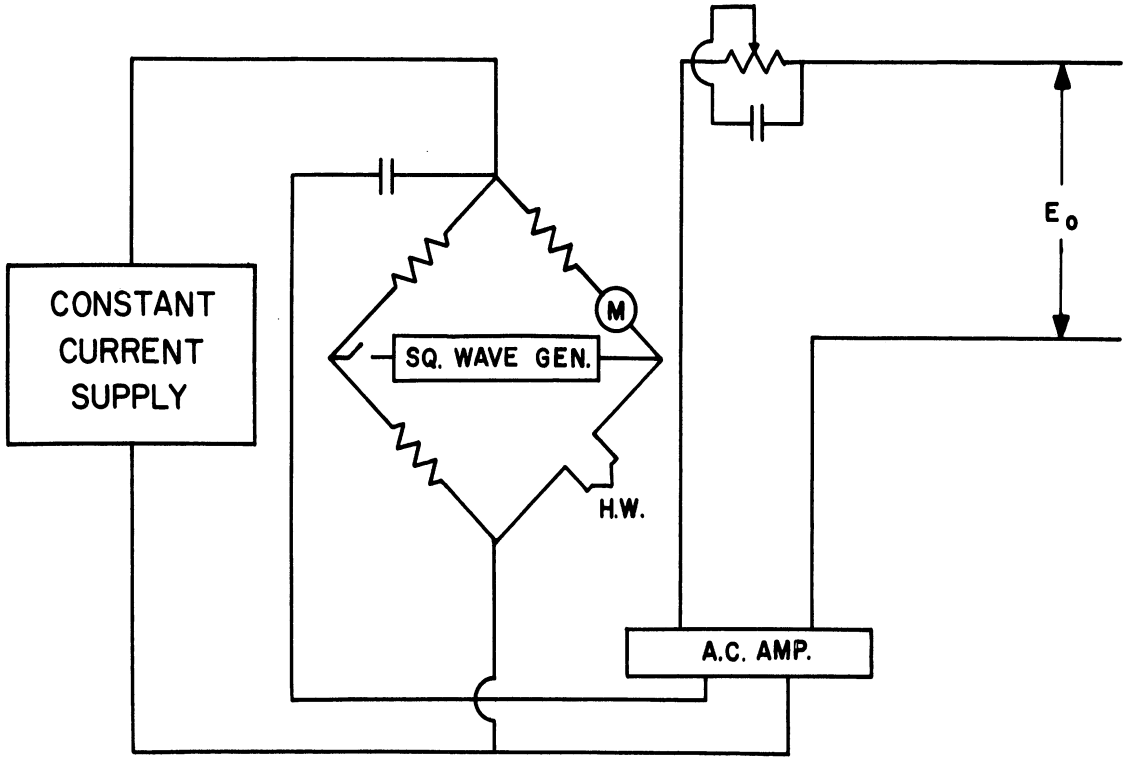

TYPICAL BAND : 2 cps TO 100 K.C.

TYPICAL NOISE LEVEL (% OF AVE. VEL.) : .01 % / 10 K.C.

Figure 2-2. The compensated constant current hot wire anemometer. The hot wire is shown as one arm of the Wheatstone Bridge.

CONSTANT RESISTANCE

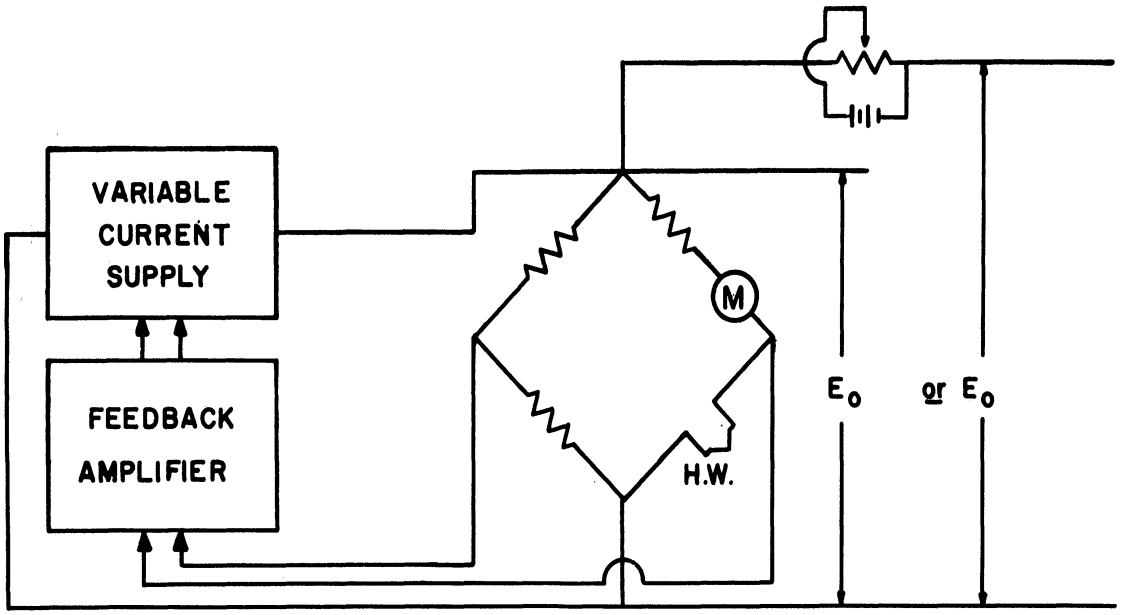

TYPICAL BAND: D.C. TO 50 K.C.

TYPICAL NOISE LEVEL (% OF AVE. VEL.): 0.1 % / 10 K.C.

Figure 2-3. The constant resistance (temperature) hot wire anemometer. The hot wire is shown as one arm of the Wheatstone Bridge.

CONSTANT RESISTANCE RATIO

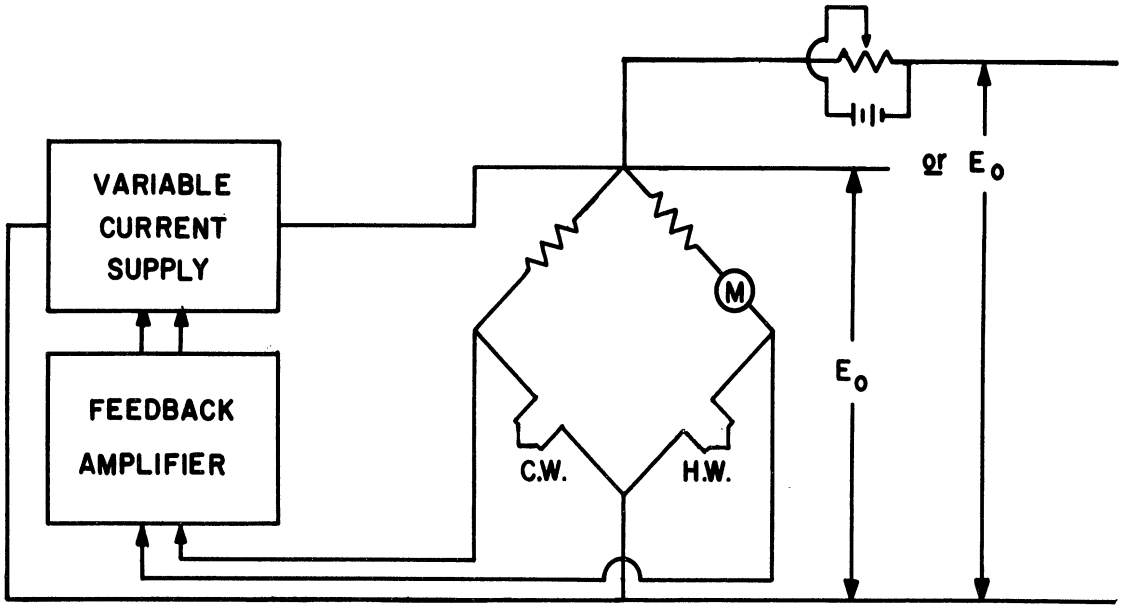

TYPICAL BAND: D.C. TO 10 K.C.

TYPICAL NOISE LEVEL(% OF AVE. VEL.): 0.1 % / 10 K.C.

Figure 2-4. The constant resistance ratio hot wire anemometer. The hot wire is shown as one arm, and the unheated wire as another arm of the Wheatstone Bridge.

automatically maintained constant by electronic feedback circuits. The hot wire heating current depends on the cooling velocity in this case, and air temperature effects are minimized. Thus as the air temperature fluctuates the unheated wire follows the temperature fluctuations and 'filters' them out of the output signal. Therefore, the output signal is nearly independent of temperature fluctuations and is a measure of air velocity only.

In practice, it is possible to attain better resolution of a low intensity of turbulence with the "uncompensated constant current" circuit, and faster response to high turbulent intensities by using either the "compensated constant current" circuit or the "constant resistance" circuit. But these alternative circuits are sensitive to air temperature changes; typically a $5^{\circ}F$ change in air stream temperature may produce a 5% error in the velocity reading. Of course, manual controls can be provided to permit readjusting the operating resistance of the wire when the stream temperature shifts from steady state level to a new one, to compensate for the air temperature change. When these circuits are used to measure instantaneous velocity in an unsteady flow in which the temperature is

fluctuating by more than a few degrees, then either the hot wire must be operated at a very high temperature, or temperature fluctuations must be measured independently in order to determine corrections. It can be shown that the hotter the wire, the smaller the errors due to air temperature change.

There are many advantages and disadvantages associated with the different modes of operation - constant current and constant temperature. Two serious limitations of the constant current method are the difficulty of determining the proper degree of compensation required and the necessity to readjust the compensation for each change in mean speed. These difficulties associated with the compensating procedure of constant current operation are, of course, completely circumvented in the constant temperature method. Indeed, an outstanding feature of the latter method is that the hot wire can be repositioned in a non-uniform flow field without additional adjustment of any of the electrical components.

On the other hand, the constant temperature method suffers from an inherently higher noise level, originating mainly in the feedback circuit, and as a consequence the

minimum value of turbulence intensity that it can resolve is higher than the corresponding value for the constant current method. The noise level, in general, is significant only in the measurement of turbulence of very low intensity, i.e., for fluctuations whose values are less than about 0.1% of the mean velocity, and in the determination of quantities which involve differentiation of the hot wire signal. The constant temperature equipment needs a separate feedback power amplifier for each wire, whereas the signals from constant current wires can be mixed before entry into a common amplifier and compensator, providing that the two wire time constants are within the accuracy required (usually about 5%). The constant temperature mode has much less change in wire sensitivity with change in operating position, and the output can be linearized by a suitable function generator to make the effective sensitivity constant.

The output of the constant current anemometer cannot be properly linearized because the wire time constant as well as the sensitivity change with the wind speed and temperature. Its use, therefore, is restricted to low intensity turbulence. The maximum permissible intensity depends on the quantities to be measured (the root-mean-square value

may be less sensitive to distortion than the frequency spectrum, for instance) and the accuracy required. The commonly accepted value for valid measurements is for the standard deviation of the fluctuations to be less than about 10% of the mean flow although this varies somewhat depending on the desired results. The advantages and disadvantages of the various methods of hot wire operation are summarized in Table 2-1.

In the atmosphere the intensity of turbulence can become large near the ground and a time scale is necessary to define a mean flow. It is obvious from the above considerations that the mode of operation required for atmospheric work is the constant temperature mode. From the two types available the one better suited for more general use is the "constant resistance ratio" since this measures velocity directly without incorporating temperature fluctuations in the output. At this time, however, the state of the art for the "constant resistance ratio" method is not sufficiently advanced for atmospheric measurements. For this reason "constant resistance", hereinafter referred to as constant temperature, equipment was used.

The design is complicated because hot wire anemometers

Table 2-1

Summary of advantages and disadvantages associated with the constant current and constant resistance modes of hot wire operation.

CONSTANT CURRENT	CONSTANT RESISTANCE	
Either compensated or uncompensated.	Constant temperature.	Constant resistance ratio.
Advantages		
1. very low noise. 2. capable of very high frequencies. 3. signals may be mixed before entry into a common amplifier.	1. capable of fairly high frequencies. 2. no compensation required. 3. can be linearized independent of wind speed fluctuations.	1. no compensation required for change in mean ambient temperature. 2. can be linearized independent of temperature fluctuations.
Disadvantages		
1. sensitive to air temperature changes. 2. difficult to determine proper degree of compensation. 3. compensation must be readjusted for each change in mean wind speed. 4. the error in linearizing increases as amplitude of wind speed fluctuations increases.	1. higher noise level. 2. separate feedback amplifier required for each wire.	1. sensitive to air temperature changes.

are low impedance (typically 5-50 ohms) devices demanding high currents (20-200 ma) and vacuum tube circuits are insufficient. Large voltage gains are required and in general no solution with only two stages of amplifiers has been possible. If more than two stages are used, on the other hand, the condition for avoiding electrical instability is quite critical. With the use of transistors, however, the impedances of wire and amplifier are more easily matched and a solution with only two amplifying stages became feasible.

2.2.1 Model M-5 Hot Wire Amplifier Unit

The equipment selected for this study was the Model M-5 Hot Wire Amplifier Unit designed by Kovasznay (1963). It is shown in figure 2-5 and the circuitry is shown in figure 2-6.

The unit is a closed loop feedback system (recall figure 2-3) which can be broken down into three parts:

1. Bridge circuit,
2. Power amplifier,
3. High gain differential amplifier.

The hot wire and a 75 ohm resistor form one section of

Figure 2-5. The model M-5 hot wire amplifier unit.

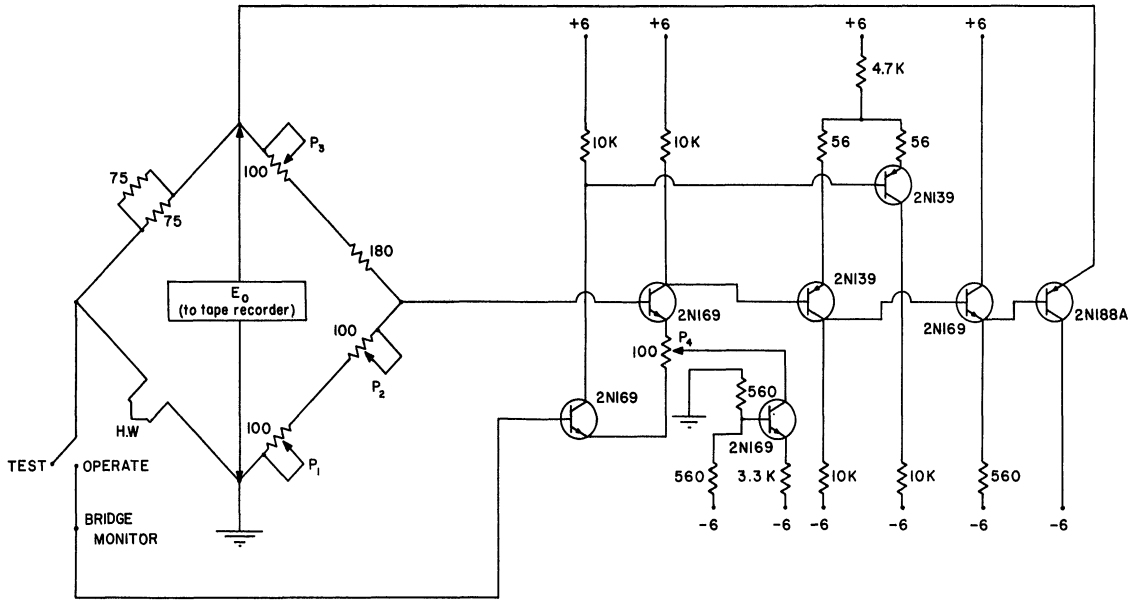

Figure 2-6. The wiring diagram for the model M-5 hot wire amplifier unit.

the bridge circuit with a second 75 ohm resistor that can be put in parallel with the first one to halve the range for hot wire resistance values. This gives a resistance range for using hot wires of 10-50 ohms. The maximum wire current is 90 ma and the output signal is of the order 0-4 volts (dependent on wire used). The other section of the bridge circuit contains the main variable resistor with a calibrated dial for setting the desired hot wire resistance, and two variable trim resistors. The trim resistors permit the bridge circuit to be adjusted for variation in component values. Connections to the bridge circuit permit the balance to be monitored during operation.

The power amplifier consists of a 2N188A transistor driven directly by a 2N169 transistor operating as an emitter follower. The 2N188A is connected as an emitter follower also and the bridge circuit acts as the emitter resistor.

The high gain differential amplifier is a two-stage unit in which current through the first stage is kept constant by a 2N169 transistor to improve the common mode signal rejection. Each of the two 2N169 transistors in the first stage is directly connected to a section of the bridge

circuit as the input to the amplifier. Connections are made to both amplifier outputs for checking the balance and voltage level. One of the outputs is connected to the driver of the power amplifier. The four main transistors of the differential amplifier are enclosed in a thermal shield to insure that all are subject to the same ambient temperature conditions. The 2N169 transistors in the first stage are matched to within 3% for values of β and base-emitter voltage vs. collector current, where β is a characteristic parameter associated with transistors.

2.2.2 Hot Wire Probes

Two Flow Corporation X-type hot wire probes were used with the hot wire amplifier units. These are Model HWP-X-W12X-L24 with two tungsten hot wire filaments mounted 90^{o} to each other and 0.03 in apart (figures 2-14 and 2-15). The filaments are 0.1 in long and 0.00015 in in diameter giving a length to diameter ratio of 667. The typical time constant for this filament is 0.0004 sec.

The rate of heat loss is determined mainly by the velocity component perpendicular to the wire. The effect of the velocity component parallel to the wire becomes

noticeable only when the normal velocity component is very small or zero. The equation for the effective velocity as seen by the wire is given by Hinze (1959) as

$$U_{eff}^2 = U^2(\sin^2 \varphi + C \cos^2 \varphi) \qquad 2\text{-}1$$

where φ is the angle between the wind velocity vector and the wire, and C is a factor varying between 0.1 and 0.3 depending on the magnitude of the velocity. The value of C increases with decreasing velocity. For the practical range $20^\circ < \varphi < 90^\circ$, only the first term of equation 2-1 is retained so that

$$U_{eff} = U \sin \varphi. \qquad 2\text{-}2$$

Another equation valid for angles of φ between 5° to 90° is given by Flow Corporation Bulletin No. 47B (1963) as

$$U_{eff} = U \sin \varphi \left[1 + 1.2 \, (D/L)^{1/2} \cos^2 \varphi\right] \qquad 2\text{-}3$$

where D is the wire diameter and L is the wire length. As pointed out above, the diameter to length ratio for this case is 1/667, so that the value of $1.2(D/L)^{1/2}$ is 0.05. If the second term in the brackets is considered small compared to 1, then equation 2-3 reduced to equation 2-2. Equation 2-2 is used hereinafter for computing the velocity.

When two wires are mounted normal to each other the two components of the wind speed can be obtained in the plane formed by the wires.

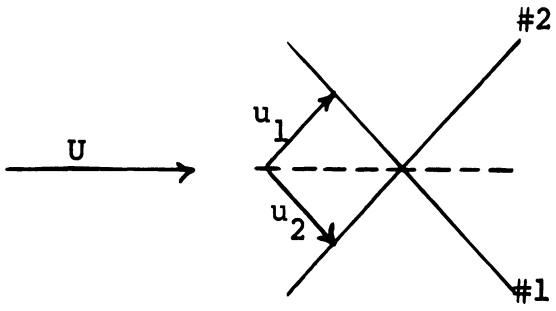

Figure 2-7. Diagram illustrating wind components as sensed by the X-probe.

This is illustrated in figure 2-7 for two-dimensional air flow. Since wire #1 measures the u_1 component of U and wire #2 measures the u_2 component of U, then U can be calculated as

$$U = (u_1^2 + u_2^2)^{1/2}. \qquad 2\text{-}4$$

By mounting another X-probe in a plane normal to the horizontal X-probe, the vertical component of the wind can be measured. The exact configuration used is shown in figure 2-14 and described in detail in the section on field measurements (section 2-5).

2.3 Calibration of the Hot Wire Anemometers

The calibration of the hot wire anemometers was a

major problem. The problem of calibration caused much added work in the data reduction and analysis phases as pointed out in Chapter III. In the beginning it was thought that the wires could be calibrated by wind tunnel techniques and then taken to the field with a portable wind tunnel for periodic recalibration. However, this was not practical because of the changing characteristics of the wires in atmospheric flows. The basic hot wire equations are derived below and from the equations a calibration technique is determined.

The hot wire equations can be represented in a simple form. First, the linear dependence of electrical resistance on temperature is assumed:

$$R = R_o (1 + a) \qquad 2\text{-}5$$

with $a = \alpha(T - T_o)$

where α is the temperature coefficient of resistivity for the wire,

T operating temperature of the wire,

T_o reference "cold" temperature (by definition the temperature assumed by the unheated wire exposed to the air-stream).

Next, the heat loss of the wire is assumed to follow

the well-known King's law (1914):

$$H = (T - T_o)(B\sqrt{U} + C). \qquad 2\text{-}6$$

King's law is reasonably well-obeyed in incompressible flow (Mach number less than 0.2 - 0.3) and for Reynolds numbers larger than 0.1; conditions which are effectively satisfied in the atmosphere near the ground. For convenience, the constants in equation 2-6 will be replaced by constants having the dimensions of velocity and electrical current:

$$H = 2aI_o^2 R_o \left(\sqrt{\frac{U}{U_o}} + 1\right). \qquad 2\text{-}7$$

The input of heat is electrical and is given by:

$$W = I^2R = I^2R_o(1 + a) \qquad 2\text{-}8$$

from equation 2-5.

For static equilibrium, we have H = W and setting equations 2-7 and 2-8 equal to each other the non-dimensional form of the hot wire equation becomes:

$$\frac{I^2}{I_o^2} = \frac{2a}{1+a}\left(\sqrt{\frac{U}{U_o}} + 1\right). \qquad 2\text{-}9$$

Rewriting equation 2-9 and solving for U, the following is obtained:

$$U = U_o \left(\frac{1 + a}{2aI_o^2} I^2 - 1\right)^2. \qquad 2\text{-}10$$

The assumption of static equilibrium is justified since the M-5 hot wire amplifier is capable of responding to 50 KC which is much faster than any fluctuations expected in the atmosphere.

Since the resistance of the system is held constant, with an appropriate change in constants equation 2-10 can be written in terms of voltage instead of current. This is necessary since the tape recorder is a voltage recording system. Then the wind speed can be expressed as a function of the voltage drop across the bridge:

$$U = U_o(MV^2 - 1)^2 \qquad 2\text{-}11$$

where $M = \frac{1 + a}{2aV_o^2}$.

Equation 2-11 is the form of the equation used in linearizing the voltage measured and obtaining the desired wind speed.

To find the values of the constants M and U_o in equation 2-11, wind tunnel tests were conducted at various temperatures. The wind tunnel in the Meteorological Laboratories which is located in an unheated room was used. A range of temperatures was obtained by making early morning tests and afternoon tests.

Another wind tunnel located in the Fluid Laboratories at North Campus was used to make several tests. Heating coils mounted at the tunnel intake were varied electrically, thereby allowing tests over a range of temperatures.

Since many data points were obtained during each test, statistical methods were used to calculate the desired constants. Least square methods were used after equation 2-11 was reduced to a linear form. This was accomplished as follows: Recall equation 2-11

$$U = U_o(MV^2 - 1)^2. \qquad 2\text{-}11$$

Expanding gives

$$U = U_o M^2 V^4 - 2U_o MV^2 + U_o \qquad 2\text{-}12$$

which may be rewritten by making the following transformation:

$$A = U_o M^2,\ B = -2U_o M,\ C = U_o,\ \text{and}\ X = V^2$$

and gives

$$U = AX^2 + BX + C. \qquad 2\text{-}13$$

In order to determine the values of the constants in equation 2-13 from the data,

let $x = X + x_o$

and $u = U + u_o$

where x_o and u_o are any corresponding values of x and u taken from the data. Equation 2-13 becomes

$$U + u_o = A(X + x_o)^2 + B(X + x_o) + C$$

$$= (Ax_o^2 + Bx_o + C) + (B + 2Ax_o)\, X + AX^2$$

and therefore

$$U = (B + 2Ax_o)\, X + AX^2 \qquad 2\text{-}14$$

since $u_o = Ax_o^2 + Bx_o + C$. Dividing equation 2-14 by X and defining the transformation $Y = U/X$ gives:

$$Y = AX + (B + 2Ax_o). \qquad 2\text{-}15$$

Equation 2-15 represents a straight line between X and Y with the slope of the line given by A and the intercept by $(B + 2Ax_o)$. For equation 2-15 the data could be analyzed with the method of least squares and values of the coefficients were determined. After values for A and B were determined, C was evaluated by an averaging process by recalling $C = u_o - Ax_o^2 - Bx_o$ and using all the data points for u and x.

Several internal checks were available since $A = B^2/4C$. Since $M \approx 1$, then $A \approx -1/2B$ and $A \approx C$. M is a parameter that is controlled by a dial setting on the hot wire amplifier and is set to one at the ambient temperature during the start of the run. With M = 1, then the output voltage at zero wind speed is -1 volts; this condition satisfies equation 2-11.

Table 2-2 gives six sets of values for several different temperatures. The coefficients for the quadratic equation 2-13 are given as well as M and V_o^2, where V_o^2 is a constant in M. The value of U_o is given by C and since the probe has two wires, values are given for each wire.

Table 2-2

Coefficients for the hot wire equation 2-13 and other constants used in equation 2-11.

$\bar{T}(^oF)$	A	B	C	M	V_o^2	a
82.3	25.8	-52.0	26.1	1.002	1.608	0.45012
	30.3	-62.5	31.3	1.008	1.599	0.45011
76.1	11.9	-24.6	12.3	1.009	1.597	0.45008
	11.6	-23.7	11.9	1.006	1.602	0.45009
61.2	13.7	-30.5	15.3	1.026	1.570	0.45008
	14.9	-31.9	16.0	1.017	1.584	0.45008
66.4	8.3	-11.3	5.7	0.910	1.770	0.45009
	10.0	-15.8	7.9	0.942	1.710	0.45013
66.2	17.1	-34.4	17.2	1.002	1.609	0.45008
	16.6	-31.4	15.7	0.985	1.635	0.45011
64.5	16.5	-32.9	16.5	0.999	1.612	0.45007
	15.6	-28.8	14.4	0.980	1.644	0.45008

$\bar{T}$ is given in ^oF, A, B, and C are in ft/sec; M is in volts^{-2} and V_o is in volts. Recall $U_{o_2} = C$ and $A \sim C$ and $B \sim -2C$, $a = \alpha(T-T_o)$ and $M = 1 + a/2aV_o^2$. Values are given for each wire on the X-probe.

As seen from Table 2-2, the values for U_o range from about 5 to 31 ft/sec. As a possible means of describing U_o as a function of temperature, a graph of U_o vs. $\bar{T}$ is given in figure 2-8. There are two regions on the graph with the division at 66.3°F. It is seen that the calibrations of the two wires do tend to change together indicating that what affects one wire also affects the other wire. In general, no relationship is apparent for U_o from the parameters measured. U_o is believed to be a function of the physical characteristics of the wire determined by the aging affect on the wire. This aging affect is caused by such diverse quantities as pollen in the air, humidity, burning of pollutants by the wire, oxidation of the wire, the exhaust from airplanes taking off upwind at Willow Run Airport (where the field experiments were conducted), and perhaps a dozen more parameters that are uncertain or unknown.

With this apparent inconsistency in U_o, the best approach was to use the wind profile measured in the field to calibrate the hot wires. The technique was to use the wind profile determined by the three-cup anemometers, select the height at which the hot wires were operating (in most cases 1 meter), evaluate the wind speed and determine U_o.

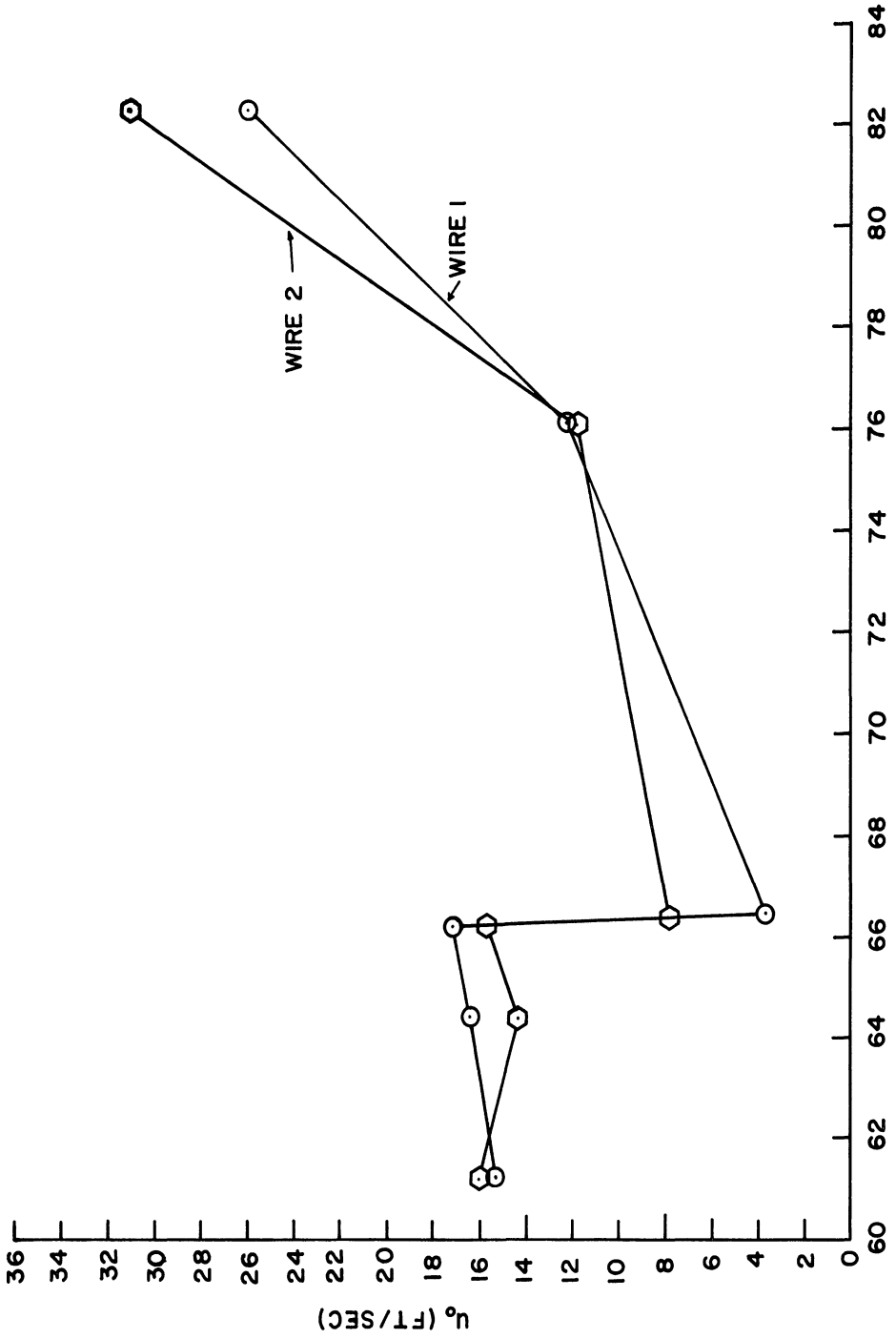

Figure 2-8. A plot of U_o vs. T where U_o is in ft/sec and T in °F.

By computing from the output the quantity $\overline{(MV^2-1)^2}$ and dividing by the wind speed obtained from the profile averaged during the same period of time, the resultant is U_o. Recalling equation 2-11 and solving for U_o; one gets

$$U_o = \frac{U_{cup}}{\overline{(MV^2-1)^2}} \cdot \qquad 2\text{-}16$$

Thus a U_o is determined for a certain interval and assumed constant during that interval.

2.4 Error Analysis for Data Collection

In any program the reliability of the data must be known in order to assess the degree of confidence that can be placed in the final analysis. A systematic evaluation of the possible errors is broken into three main groups for analysis: 1) Data Collection, 2) Data Reduction, and 3) Data Analysis. This section concerns itself with the first - the error analysis in data collection.

The first consideration in this respect is the instrumentation response. As was shown earlier the electronic feedback loop has a response of 50,000 cps so that any frequency errors in electronic feedback can be neglected. This was part of the basic assumption used earlier to justify

static equilibrium in the derivation of the hot wire response (equation 2-11).

A second consideration in instrumentation response is the time constant (or response time) of the sensing element. The hot wires were described earlier and it was pointed out that they respond to frequencies of 2,500 cps with a time constant of 0.0004 sec. In this respect frequency errors can be neglected since at these high frequencies the energy of the turbulence fluctuation is small.

The most important unknown in equation 2-10 is U_o which contains the unknown parameters in the response of the hot wire element. Fortunately, U_o is a linear variable so that it introduces only linear errors. A non-linear error is introduced into the calculation of U by the fluctuating air temperature. The air temperature is a measured quantity, however, and can be taken into account in the data reduction. For the analysis presented in Chapter IV, nevertheless, the temperature correction was assumed small and was not taken into account in the calculations.

The error due to temperature changes may be calculated with equation 2-11. Since temperature enters as a squared term in equation 2-11 and voltage is a fourth power term,

both variables need to be used. Table 2-3 gives the results of an error analysis for both temperature fluctuations and wind speed.

The numbers in Table 2-3 give the percent error as the temperature difference varies for different wind speeds. As would be expected at higher wind speeds the voltage output is greater so that for a given temperature fluctuation the error is smaller. It can be seen from Table 2-3 that for a + 1°C change in the temperature, the error decreases from -4.9% to -2.4% or a reduction of more than half as the wind speed increases from 2.5 ft/sec to 30 ft/sec. During actual field operations temperature fluctuations amount to only a degree or two and the error is probably less than 5% most of the time. However, due to the method of calibration, with new coefficients evaluated every few minutes, the long-term error arising from the change in temperature is eliminated. Thus, only short-term fluctuations contribute to this error. These fluctuations are usually less than a degree and seldom more than a few degrees so that the error introduced by temperature changes is small.

Table 2-3

Percent error in wind speed given as a function of temperature fluctuation and wind speed.

wind speed ft/sec	2.5	5	7.5	10	12.5	15	20	25	30
^{o}C									
-10	43.9	35.8	32.0	29.6	28.0	26.8	25.1	24.0	23.1
- 7.5	33.9	27.4	24.4	22.5	21.3	20.4	19.0	18.2	17.5
- 5	23.2	18.6	16.5	15.2	14.4	13.7	12.8	12.2	11.8
- 4	18.7	15.0	13.3	12.3	11.6	11.0	10.3	9.8	9.4
- 3	14.2	11.3	10.0	9.2	8.7	8.3	7.8	7.4	7.1
- 2	9.6	7.6	6.7	6.2	5.8	5.6	5.2	4.9	4.7
- 1	4.9	3.8	3.4	3.1	2.9	2.8	2.6	2.5	2.4
0	0	0	0	0	0	0	0	0	0
1	- 4.9	- 3.9	- 3.4	- 3.1	- 3.0	- 2.8	- 2.6	- 2.5	- 2.4
2	- 9.9	- 7.8	- 6.9	- 6.3	- 5.9	- 5.7	- 5.3	- 5.0	- 4.8
3	-15.0	-11.8	-10.3	- 9.5	- 8.9	- 8.5	- 7.9	- 7.5	- 7.2
4	-20.2	-15.8	-13.9	-12.7	-12.0	-11.4	-10.6	-10.0	- 9.7
5	-25.4	-19.8	-17.4	-16.0	-15.0	-14.3	-13.3	-12.6	-12.1
7.5	-38.9	-30.2	-26.4	-24.2	-22.7	-21.6	-20.1	-19.0	-18.3
10	-52.8	-40.8	-35.6	-32.6	-30.5	-29.0	-26.9	-25.5	-24.5

Another temperature affect of concern is the overheat ratio $R/R_o = 1 + a$. (Recall that $a = \alpha(T-T_o)$.) Standard tables give α for tungsten as 0.0045 and the electronics are designed for a to be 0.45. This gives an operating temperature for the wire of 100^{o}C above the ambient air temperature. To check a the values given in Table 2-2 may be used. This was done for the six cases given and the result is shown in the last column on the right

Taking an average for these values gives a = 0.45009. Since the last figure is reaching the limit of accuracy with the decimal points carried, it is seen that the value of a = 0.45 is well justified.

The noise level of the data collection system determines the minimum amplitude of the signal that can be evaluated. Typically the noise level of the hot wire amplifiers is about a millivolt. The noise level of the tape recorder is about 1 millivolt, depending on frequency. In order to evaluate the noise level of the tape recorder, a zero level signal was recorded and then analyzed on the wave analyzer. This gave a spectrum of the noise level of the tape recorder and the wave analyzer system. Several such spectra were obtained. The noise level at each frequency was averaged and the standard deviation was computed. Figure 2-9 shows the results of this analysis. The average noise level is plotted and the 95% confidence levels (as computed from the data) around the mean are shown. No confidence levels were shown beyond 60 cps since they were so small. The energy at very low frequencies (less than 4 cps) is due to two main factors. First, this is reaching the limit of resolution of the wave analyzer; and second,

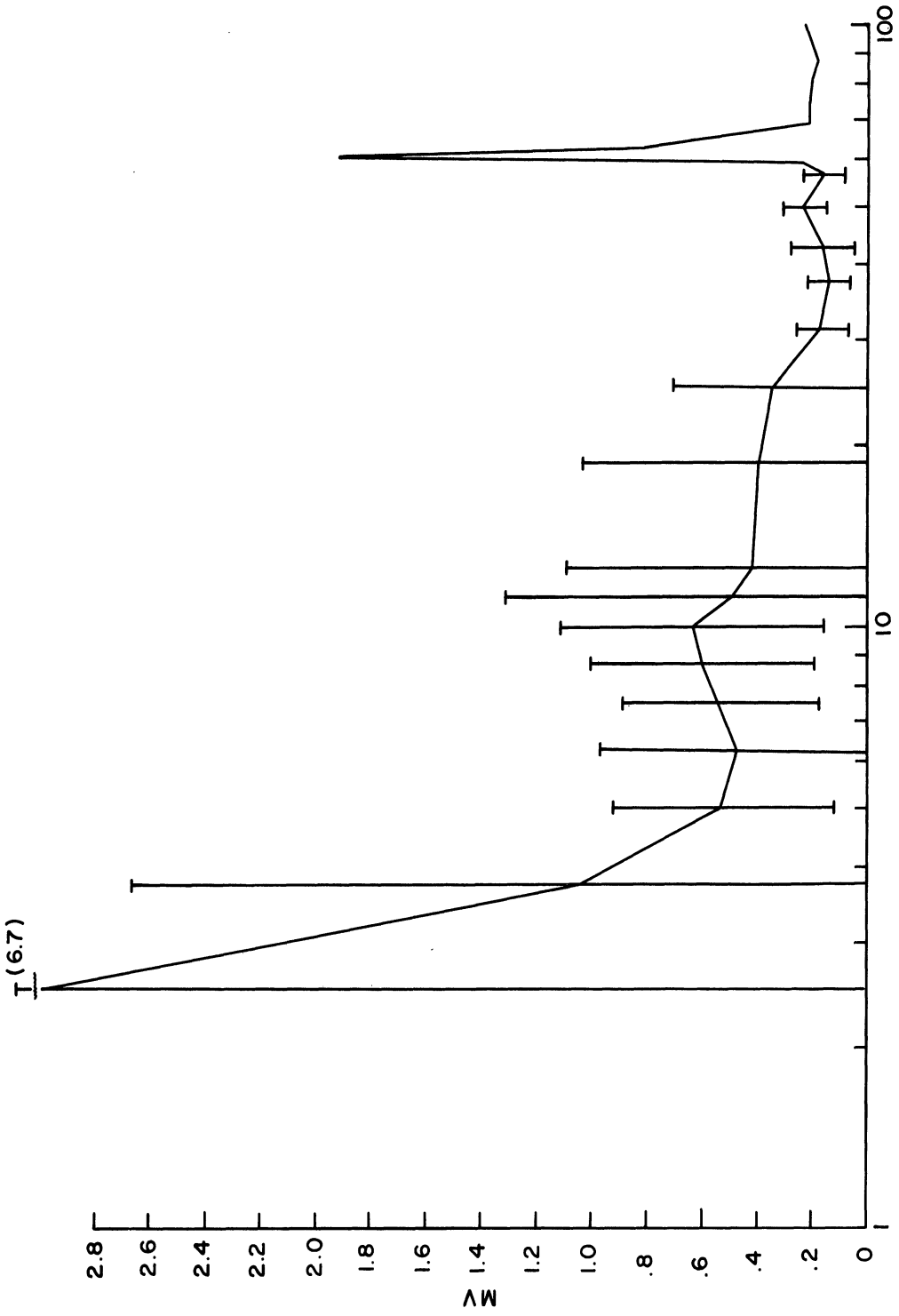

Figure 2-9. Noise level spectrum for 7-channel tape recorder and wave analyzer.

if there is any D.C. bias in the data it shows up as power in the lowest frequency. There is a small peak at 10 cps, but this is not very significant because of the wide variances in this region. Only in the region of 10 cps do the 95% confidence intervals exceed the 1 millivolt noise level. At about 30 cps the variance in the noise drops to about 0.1 millivolt and the mean level is about the same order (0.1 to 0.2 millivolts). In the region beyond 30 cps the noise level becomes largest at 60 cps where it reaches a peak of almost 2 millivolts.

The significance of the spectrum is that in the evaluation of data, the signal can be evaluated down to 0.2 millivolts with a fair degree of confidence. Since the output from the tape recorder is $\pm$ 1.4V peak-to-peak then the resolution to 0.2 millivolts gives a range of four orders of magnitude for the amplitude of the signal.

The frequency range for the analog tape recorder is 0 to 625 cps since the data were recorded at 3-3/4 inches per second. The upper limit was not checked but was accepted as correct from the specifications given by the manufacturers.

2.5 Field Measurements

The hot wire data were obtained as part of an existing program studying laser scintillation caused by atmospheric turbulence. In addition to the scintillation data, vertical profiles of wind speed and temperature were being measured to a height of four meters along the path. Temperature fluctuations were recorded to relate to the scintillation measurements. This program is described in detail by Portman, et al., (in press). To this basic experiment the addition of the hot wire anemometers was made in order to describe the three-dimensional structure of turbulence.

The data were collected at the Willow Run Airport near Ypsilanti, Michigan. Figure 2-10 shows an aerial view looking west into the airport. The test site is shown in the picture. Figure 2-11 gives a top view of the airport showing the runways and the test site. Field experiments were conducted when the wind was westerly since this offered the best fetch. From the test site to the terminal buildings on the west is about 7000 ft. As can be seen in figure 2-10 and figure 2-12 the terrain in this region is flat. Figure 2-12 shows the test site and the truck used to house the tape recorder and the electronics for the hot wire, and

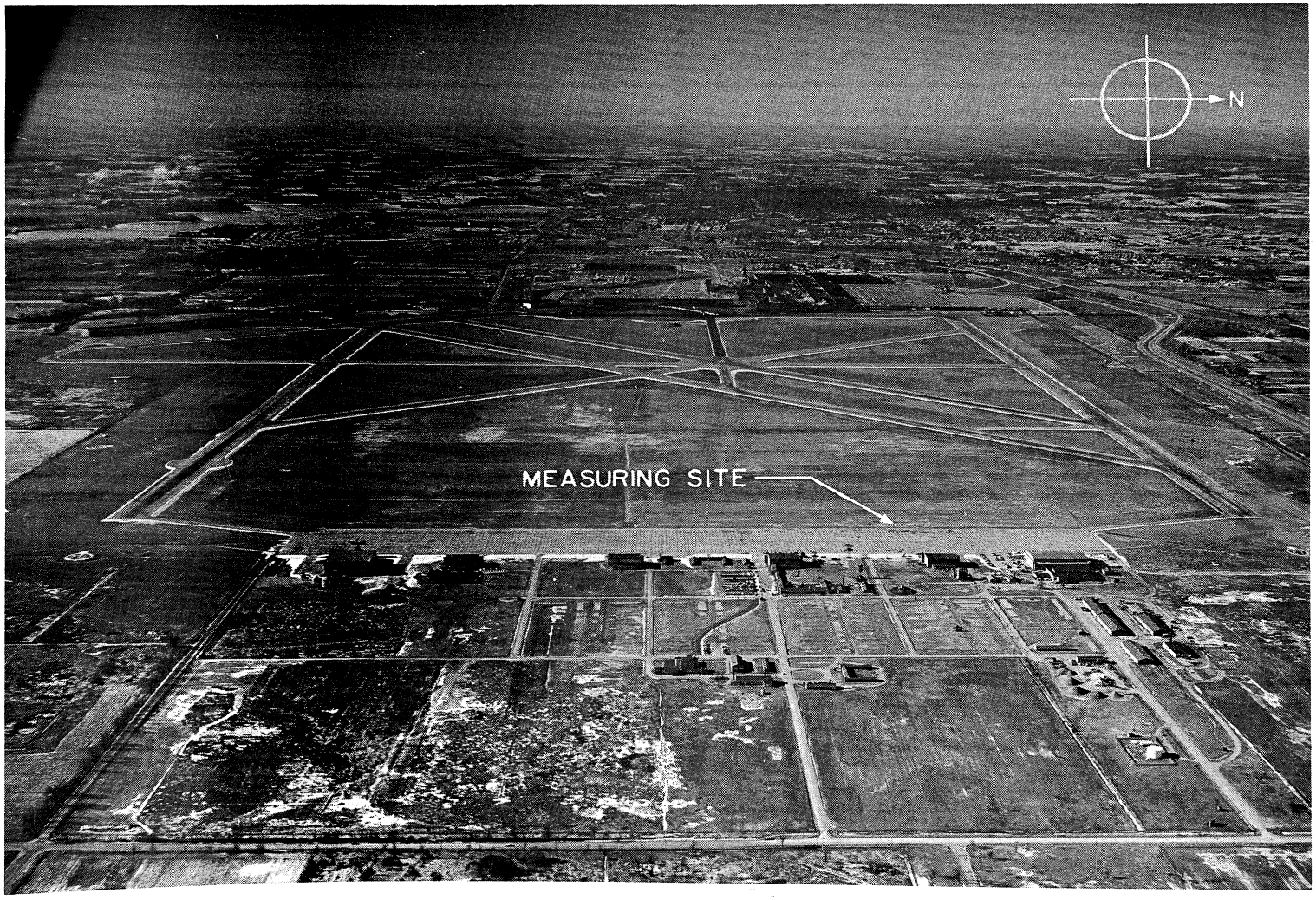

Figure 2-10. Aerial view looking west into Willow Run Airport showing location of instrument array.

Figure 2-12. View of test site and truck used to house the electronics.

profile, and scintillation measurement equipment. Just to the left of the truck and about 20 feet west, the tower with the hot wires was placed for measurement. It is not shown in the figure. Just out of the picture on the left, the 4-meter tower for the gradient measurements was located. The buildings in the left of the figure are approximately 7000 ft away. The grass was kept mowed for a distance of 500 ft upwind and the whole field was maintained in such a manner that the grass upwind (beyond 500 ft) was seldom, if ever, over two feet high.

The 3 m tower for mounting the hot wires is shown in figure 2-13. The hot wires were placed normal to each other and met at the sampling point about 8 in out to the side of the tower and several inches in front of it. The probes were mounted on a slide which could move on a rail up and down the tower so that various levels could be sampled. The probes could be lowered to a height less than a centimeter above the surface. Figure 2-14 shows a close-up of the probes and mounting bracket. The temperature sensor and a copper slug used to provide a large time constant for the reference temperature are visible. The temperature sensor is mounted such that it extends into the same

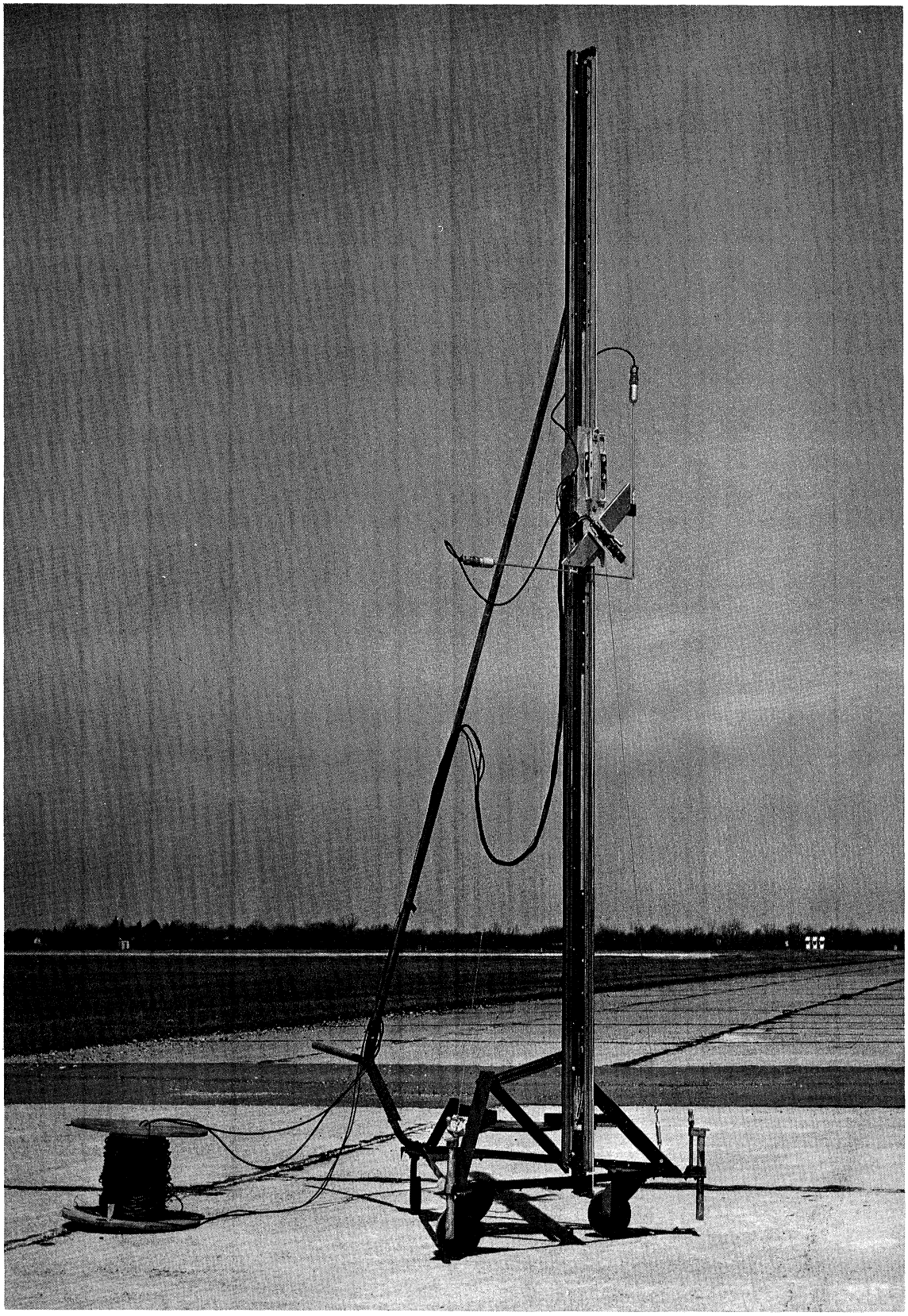

Figure 2-13. Three meter portable tower for mounting hot wire probes and temperature sensors. The probes are mounted on a rail so they can slide up and down.

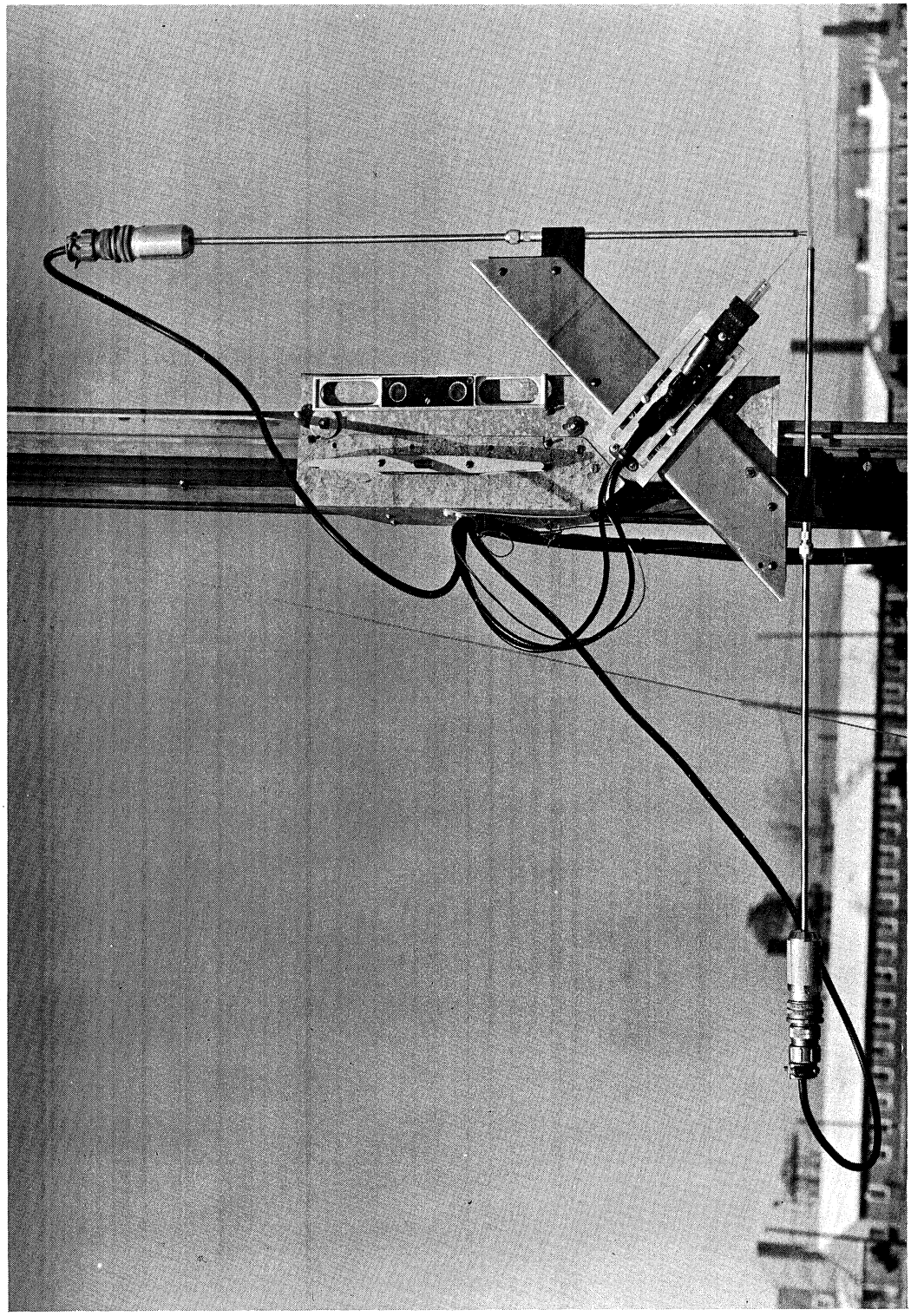

Figure 2-14. Close-up of hot wire probes, temperature sensor, and mounting bracket.

sampling space as the hot wire probes. It should be noted that the mounting bracket has two levels located on it to give some degree of assurance that the tower is level. However, due to the method of calibration described earlier, this is a second order affect.

The sampling space is shown in figure 2-15. This shows the configuration of the hot wires and the temperature sensor. The diameter of the stem of the probe is 0.25 in so that the sampling space is about 1 cm in diameter.

A carrying case was built and lined with foam padding for housing and transporting the hot wire probes with a minimum of breakage. The case and four probes are shown in figure 2-16.

The hot wire amplifiers were located in the truck. Figure 2-17 shows the four amplifiers mounted in a chassis with all the necessary control switches. The meter is used for aligning the zero calibration before each run and for monitoring the output during operation. Each amplifier requires a channel on the tape recorder so that four channels are used to obtain the hot wire measurements. The power for the amplifiers comes from batteries which supply a +6 volt and a -6 volt source.

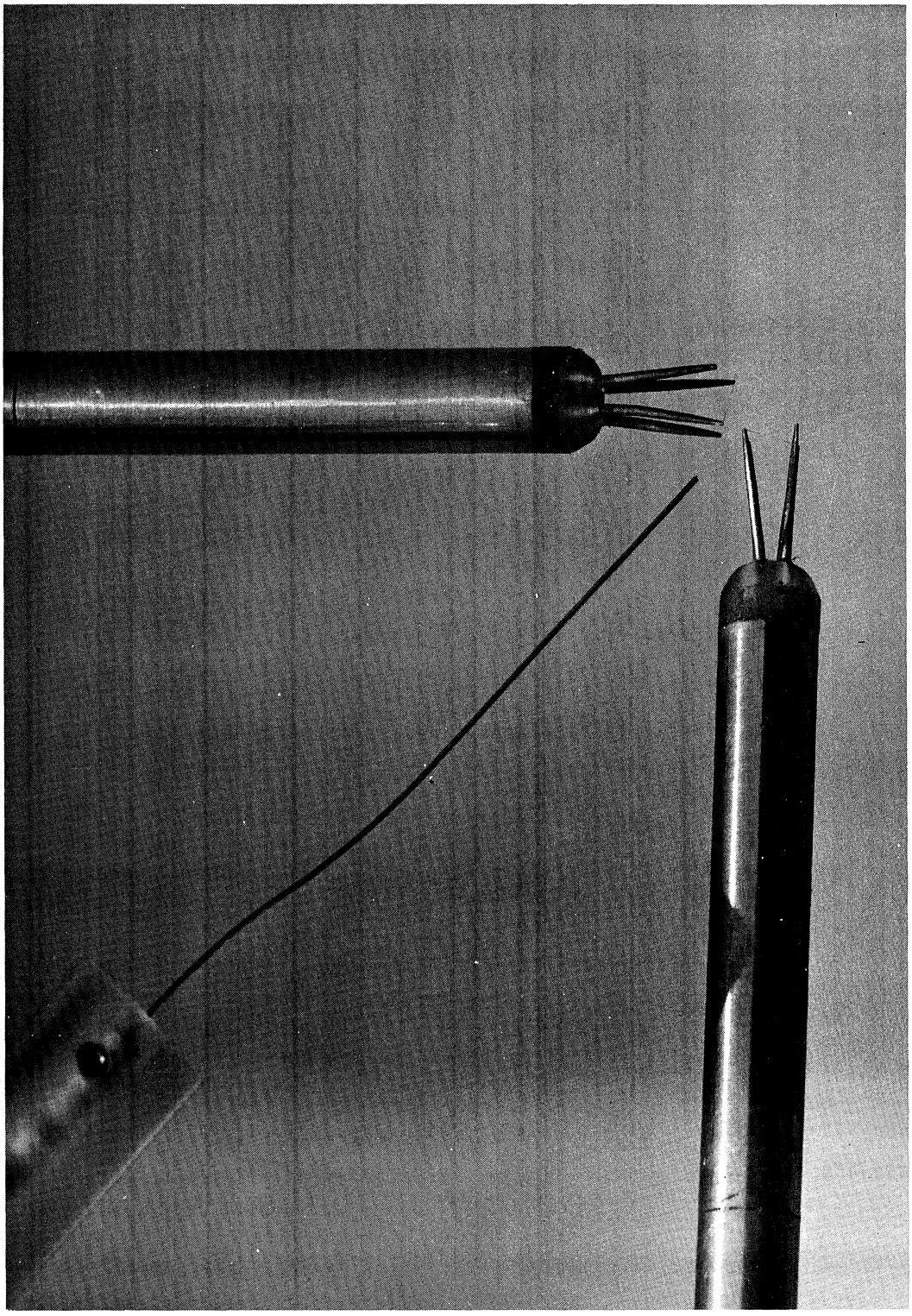

Figure 2-15. Close-up of the sampling space showing the configuration of the four hot wires and the temperature sensor. The diameter of the stem of the hot wire probe is 0.25 in.

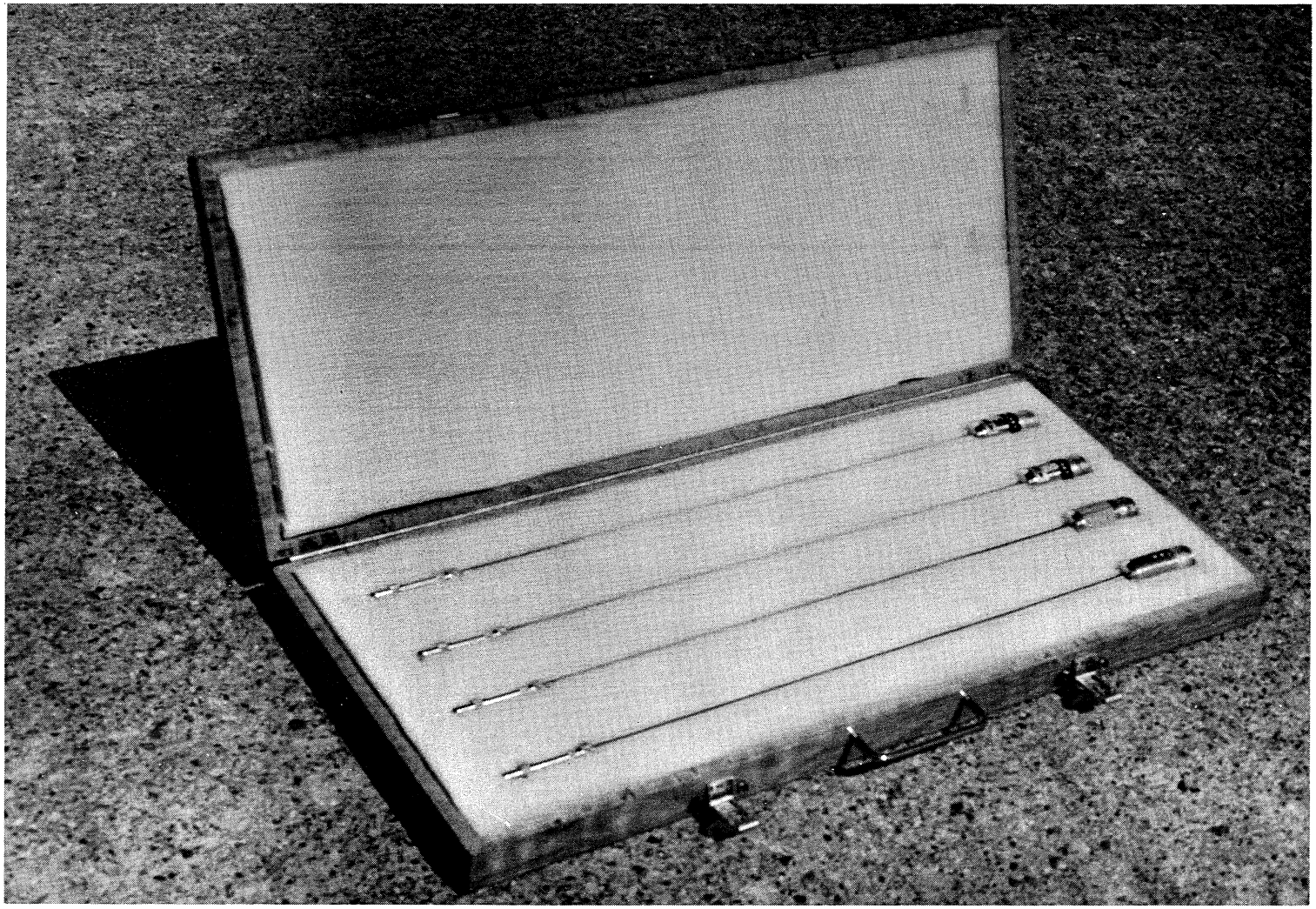

Figure 2-16. The carrying case lined with foam padding for transporting the hot wire probes.

Figure 2-17. The four hot wire amplifiers mounted on the chassis showing the necessary control switches.

For hot weather operations, a small refrigerator was modified to operate at approximately + 70°F in order to minimize thermal drift that might be experienced by the hot wire amplifiers at high temperatures. The refrigerator was mounted on wheels so that it could be easily handled and moved for field operations. As a means of preventing rapid warm air influx when the door was opened, the refrigerator was remounted on its back so that access was achieved through the top. This, of course, necessitated remounting the motor so that it operated in the proper position.

All seven channels of the tape recorder were used: four for the hot wire amplifiers; one each for temperature fluctuation, scintillation, and a control channel. The control channel recorded a D.C. level whose polarity was reversed every ten minutes. This allowed for identification marks on the tape and was used to control the data processing described in the next chapters.

Chapter III

Data Reduction and Processing

3.1 Introduction

The wind components were computed after the data signal was reconstructed and calibrated. Turbulence spectra were then evaluated for each component of the wind (u, v, and w).

The equipment used was a hybrid computer system in the Department of Meteorology and Oceanography and a IBM 7090 operated by the University of Michigan. The hybrid system is seen in figure 3-1 and described in detail in the Appendix. The analog tape recorder is shown in figure 3-1 on the table. The output jacks connect the reproduced signal into the patch board of analog console III*. The data were digitized and stored on digital magnetic tape for further processing on the 7090 computer. After u, v and w were determined by the 7090, these results were converted by the hybrid computer to an analog signal. The u, v and w signals were recorded on a tape loop recorder (figure 3-6) which allowed computing the spectrum by use of a wave analyzer (figure 3-6).

* The analog consoles are numbered at the top in the center with console III on the left, II in the center and I on the right.

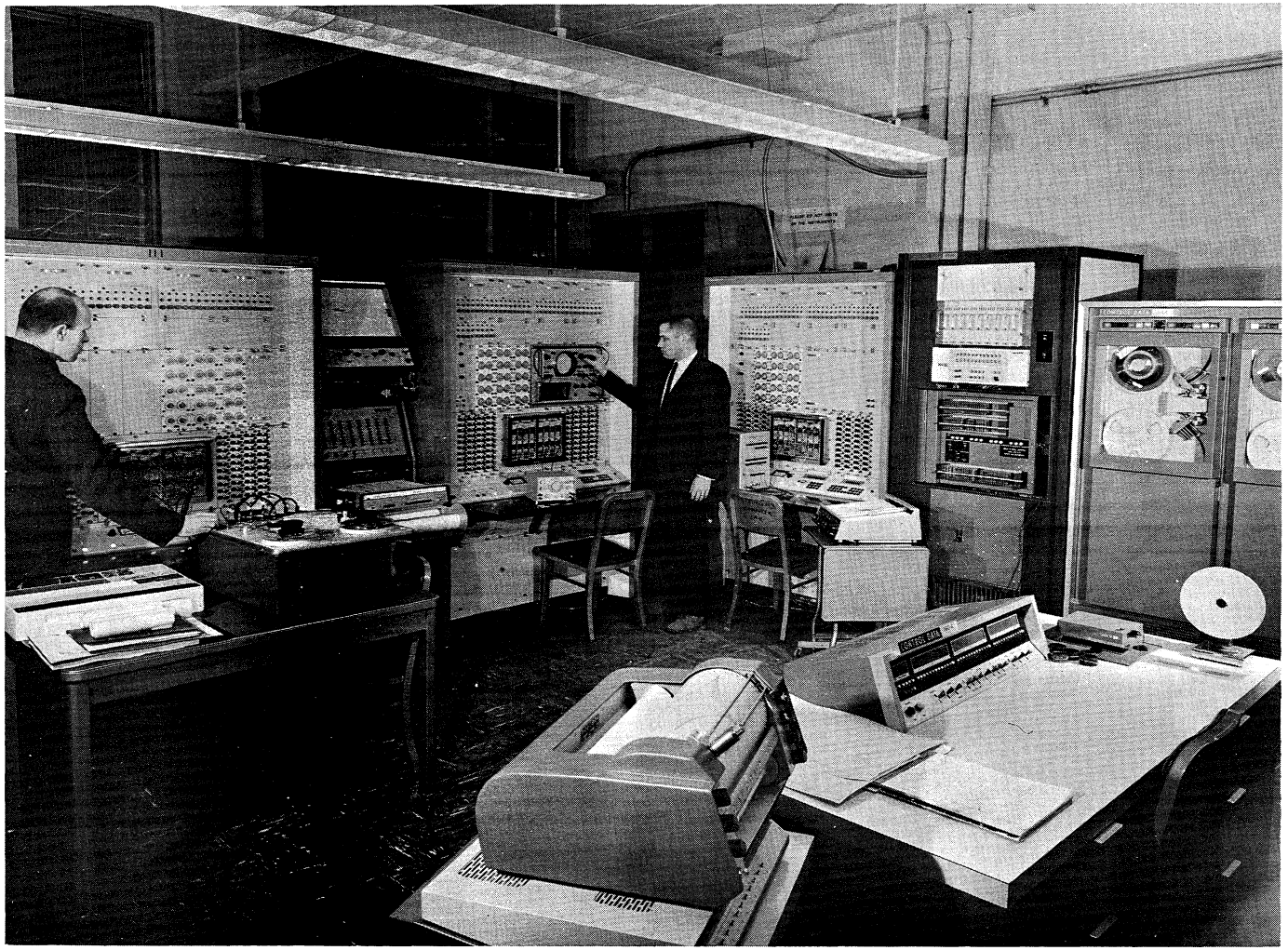

Figure 3-1. Hybrid computer system in the Department of Meteorology and Oceanography (described in the Appendix).

3.2 The Equations Used

The basic equation for the hot wire data reduction is

$$U = U_o(MV^2 - 1)^2. \qquad 2\text{-}11$$

It is used for each of the four hot wire outputs to convert voltages to velocity.

In order to determine the horizontal wind, U_H, from the two wires in the x-y plane, let us define the wind components measured by the two wires as u_1 and u_2 (figure 3-2). The two components u_1 and u_2 are measured relative to the coordinate axis made by the hot wires. Once a mean horizontal wind is determined, it is necessary to calculate the wind components relative to the new axis defined by x along the mean horizontal wind and y normal to it.

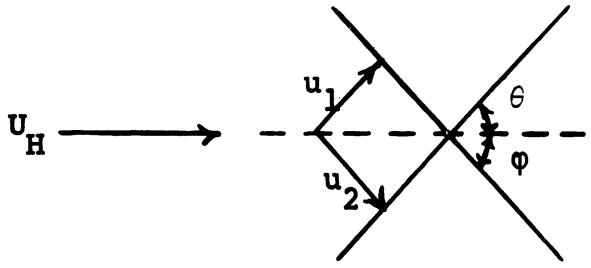

Figure 3-2. The horizontal wind components as measured relative to the hot wires.

From figure 3-2

$$u = u_1 \sin \varphi + u_2 \sin \theta \qquad 3\text{-}1$$

and

$$v = u_1 \cos \theta - u_2 \cos \varphi \qquad 3\text{-}2$$

where $\theta + \varphi = 90^{\circ}$ and u and v are the wind components relative to the mean wind coordinate system.

The values for θ and φ are determined by

$$\sin \theta = \cos \varphi = \frac{u_2}{U_H} \qquad 3\text{-}3$$

and

$$\sin \varphi = \cos \theta = \frac{u_1}{U_H} \qquad 3\text{-}4$$

where

$$U_H = (u_1^2 + u_2^2)^{1/2} \qquad 3\text{-}5$$

Equations 3-3, 3-4 and 3-5 are averaged over the interval defined by the mean wind. The results are used in equations 3-1 and 3-2 to compute u and v.

The vertical component w is computed by using the values u_3 and u_4 obtained from the wires mounted in the x-z plane.

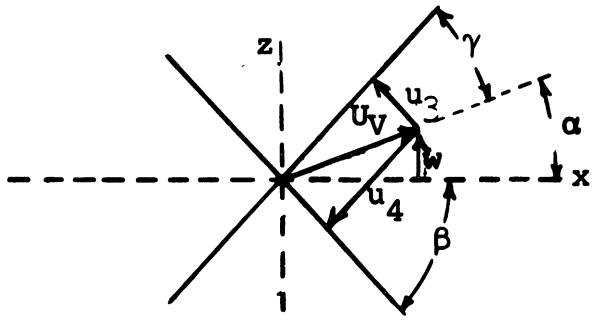

$\alpha + \beta + \gamma = 90^{\circ}$

Figure 3-3. The vertical wind component as measured relative to the hot wires.

From figure 3-3

$$w = U_v \sin \alpha \qquad 3\text{-}6$$

and

$$\cos \gamma = \frac{u_4}{U_v}; \quad \sin (\alpha + \beta) = \frac{u_3}{U_v} . \qquad 3\text{-}7$$

It follows that

$$w = U_v \sin \alpha = U_v \sin [90 - (\gamma + \beta)] =$$

$$U_v \cos (\gamma + \beta) \qquad 3\text{-}8$$

and

$$\cos (\gamma + \beta) = \cos \gamma \cos \beta - \sin \gamma \sin \beta$$

$$= \frac{u_3}{U_v} \cos \beta - \frac{u_4}{U_v} \sin \beta . \qquad 3\text{-}9$$

Substituting equation 3-9 into equation 3-8 gives

$$w = u_3 \cos \beta - u_4 \sin \beta . \qquad 3\text{-}10$$

The angle β is determined by two factors: first, the physical orientation of the wires with respect to the earth's surface, and second, the relative response of the two wires in the vertical plane. If the wires were orientated so that they made other than a 45° angle with the plane of the earth's surface then the whole system would be rotated by the increment of the angle given by the difference between the true angle and 45°. The method

used in the field to align the wires was to sight along the horizon of the earth's surface and to rotate the probe until it appeared to be 45^{o} to the horizon.

An error that could be interpreted as a rotation of the axis would occur if the two wires had different response characteristics. If u_3, for instance, gave a larger voltage than u_4 at the same wind speed, the result would be interpreted as a vertical velocity since the difference of the response of the two wires is used to obtain w.

Averaging equation 3-10 gives an expression for $\bar{w}$ if β is constant over the interval used for averaging. Use of equation 3-10 requires also constant relative calibration of the two wires. Experience has shown that what affects one wire usually affects the other wire and their calibrations do tend to change together. This is therefore not a severe restriction as long as the averaging time is not long. From experience, an interval of 10 to 15 min would not be considered too long.

If it is assumed that the average of the vertical wind is zero, the following expression is found:

$$\bar{u}_3 \cos \beta - \bar{u}_4 \sin \beta = 0$$

or

$$\frac{\bar{u}_3}{\bar{u}_4} \cos \beta = \sin \beta \ . \qquad 3\text{-}11$$

Substituting equation 3-11 into equation 3-10 yields

$$w = \cos \beta \ (u_3 - u_4 \frac{\bar{u}_3}{\bar{u}_4}). \qquad 3\text{-}12$$

Calculation of the ratio $\bar{u}_3/\bar{u}_4$ gives an indication of the relative calibration of the two wires used for obtaining w. Since the physical orientation of the probe does not change, then a time variation of the ratio $R(=\bar{u}_3/\bar{u}_4)$ would show the relative calibration shift between u_3 and u_4. Ideally R should equal unity and β should equal 45°. For the purpose of calculation β was assumed to be equal to 45° since there was no way to determine this value from the data. However, the exact value of β does not affect the shape of a frequency spectrum of w. Since both β and R are assumed constant over the interval of interest, then from a signal processing point of view, any error in β or R simply introduces a constant bias which can be removed easily in the calculations. Thus errors in β or R do not affect the relative shape of the spectrum curve as long as they are constant.

3.3 The Computer Processing

Both digital and analog equipment were used to reduce the raw data. A general diagram is given in figure 3-4 showing the various equipment used.

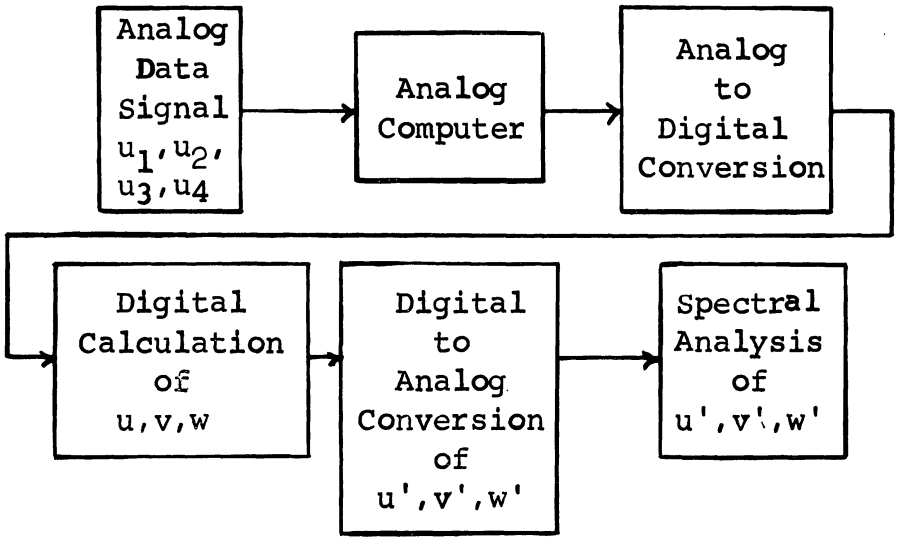

Figure 3-4. Schematic diagram showing the computer processing.

The data collected in the field were stored on analog tape in a frequency-modulated (FM) mode. They were then reproduced and played into the analog computer. The first process involved calculating calibration coefficients used to reconstruct the analog signal. Before and after each field run, calibration signals were recorded on the analog tape. The use of these calibration signals allowed reconstruction of the signal. This was required since the electronics in the tape recorder had a tendency to drift over a long period of time. Since some of the data were collected

over a year prior to analysis, reconstructing the signal to its original form was necessary.

The data were fed to the analog computer and processed with a running average of one-hundredth of a second. Exponentially-mapped-past statistics were used because only data from the present time and its recent behavior were available. This follows the development of R. M. Fano (1950), J. L. Holloway (1958), Joseph Otterman (1960) and Brock and Provine (1962). The exponentially-mapped-past statistical variables (hereinafter referred to as emp variables) are quantities relating to a set of observations computed in such a way that the recent values of the observations contribute more strongly than the values observed in the more distant past.

The emp average $\overline{f(o)}$ of a continuously-observed variable f(t) is defined as

$$\overline{f(o)} = \alpha \int_{-\infty}^{o} f(t)\, e^{\alpha t}\, dt \qquad 3\text{-}13$$

where the past extends from 0 to $-\infty$, and α is a normalized weighting function since

$$\int_{-\infty}^{0} e^{\alpha t}\, dt = \frac{1}{\alpha} . \qquad 3\text{-}14$$

f(t) is the average of f(τ), determined experimentally with information about f(t) up to the time t only. For an arbitrary moment t (value negative) in the past, the emp average is given by

$$\overline{f(t)} = \alpha \int_{-\infty}^{t} f(t)\, e^{\alpha(\tau-t)}\, d\tau =$$

$$\alpha e^{-\alpha t} \int_{-\infty}^{t} f(\tau)\, e^{\alpha\tau}\, d\tau \,. \qquad 3\text{-}15$$

This is a convolution integral of f(τ) and describes an impulse response for a low pass RC filter. This is represented by a "leaky" integrator with leakage time constant RC = 1/α. The computation of the emp average in accordance with equation 3-15 is as follows:

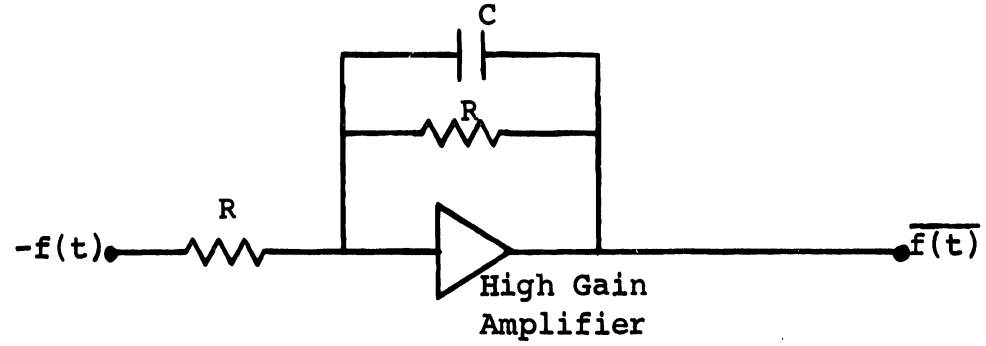

Figure 3-5. Computation of $\overline{f(t)}$ in accordance with equation 3-15.

where R and C (the resistance and capacitance) are chosen such that RC = 1/α.

The smoothing function defined above is continuous but

not an even function (it has zero values for $t > 0$) so a phase angle error is introduced into the frequency response of the running mean. It is given by $\phi = \tan^{-1}(-\frac{2\pi f}{\alpha})$.

As stated above the data were averaged with $\frac{1}{\alpha} = 0.01$ seconds. The averages were then converted to digital form at a rate of 400 points per second. A continuous input of data was achieved by using both the normal and buffer channels on the CDC 160-A computer.

The data conversion was controlled by a precision timing marker (seen in figure 3-1 on analog console I) which interrupted the digital computer for data input at specified intervals. In essence, it placed the digital computer under analog control. The timing problems were of the greatest concern in constructing the digital program for this operation because the digital machine must have completed a necessary sequence of operations and be waiting for an analog interrupt to occur.

The digital computer fed the data into the core and after a specified number had been stored, the data were transferred to digital magnetic tape. Timing was such that data transfer to tape could not be accomplished in the interval between interrupts. The buffer channel on the digital

computer was used for data transfer leaving the computer free to continue the data input while the transfer was taking place. A continuous data input was maintained then without breaks in the data conversion or transfer.

The interrupt signal was turned on and off by a relay driven by the control signal recorded on the data tape. The control signal was recorded in 10 min intervals and at a rate of 400 data points per second, a total of 20 min of data could be stored on one 2400 ft roll of tape. There were two 10 min intervals of data on each roll of digital tape. The conversion of data was a real time operation, i.e. it took 20 min of computer time to convert 20 min of data.

The digital data tapes were then taken to the University's Computing Center where they were data input tapes for the IBM 7090 computer.

Programs were written to calculate u, v, and w using equation 3-1, equation 3-2 and equation 3-10. In addition, $U_H(=\sqrt{u_1^2 + u_2^2})$, $U_v(=\sqrt{u_3^2 + u_4^2})$, and w (equation 3-12) were calculated and all of the data stored on magnetic tape. The programs were written in a compiler language which does not use the buffer systems on the 7090 so that some machine

time was used for data transfer processes. To process 12 min of data, the 7090 took approximately 40 min. Results printed out were the averages for u, v, w, $R(=\bar{u}_4/\bar{u}_3)$, U_H, U_v and w (calculated from equation 3-10).

The results tape containing u, v, and w was read by the CDC 160-A and the average subtracted from each value. The resultant values of u', v', and w' were then converted to an analog signal and recorded on the tape loop recorder/reproducer (figure 3-6) at a slow record speed. The tape loop recorder/reproducer played back the signal at a high speed and the power at each frequency was computed using a Hewlett Packard 302A Wave Analyzer. The power was then converted from millivolts to cgs units and plotted in various forms. These results are given in Chapter IV. A detailed description of the tape loop and wave analyzer system is given by Portman, et.al. (in press).

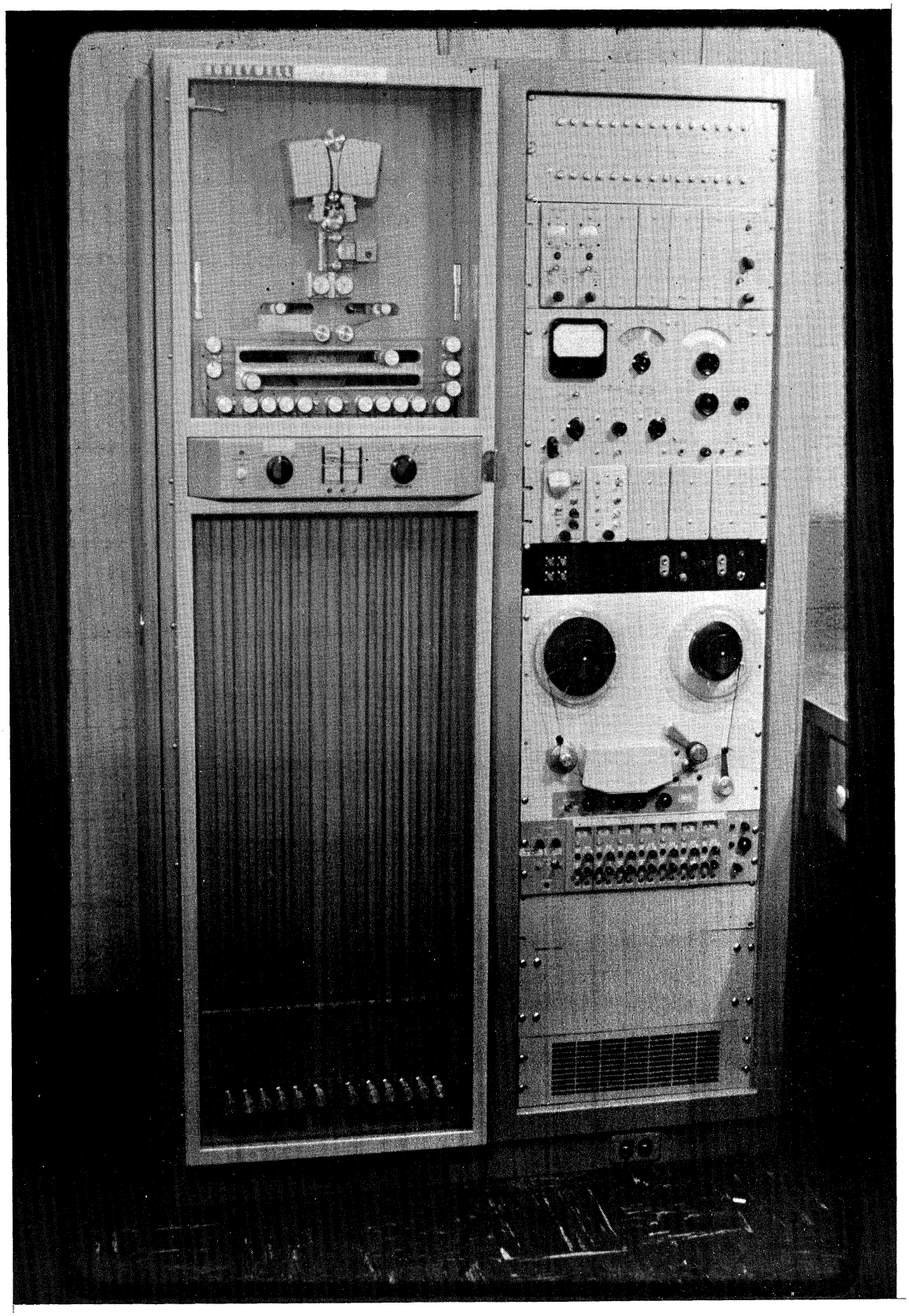

Figure 3-6. Analog tape loop recorder/reproducer, wave analyzer, and 7-channel tape recorder/reproducer.

Chapter IV

Results and Conclusions

4.1 Introduction

The equation used as a basis to test for local isotropy was given in Chapter I:

$$F_{g(r)}(f) = \frac{1}{2} F_{f(r)}(f) - \frac{f}{2} \frac{dF_{f(r)}(f)}{df} \qquad 1\text{-}8$$

Dimensional reasoning leads to a -5/3 law between the spectral function and frequency (equation 1-14) and it follows (equation 1-18) that for this case the v and w spectral functions should be equal and exceed the u spectral function by a factor of 4/3. An analysis of the data should be able to show within what bandwidth the conditions of local isotropy exist.

To establish the existence of local isotropy, however, requires knowledge about all points in space, not only that which can be obtained with the point measurements described herein. Satisfying equation 1-8 at a point in space means only that spherical symmetry exists at that point while the concept of isotropy demands spherical symmetry at all points in space. The time series data collected can be thought of as a line measurement using Taylor's assumption so the data can then be considered

measurements of a probe moving through the sample space. Since the turbulence is random, the parcel sampled could have its origin in any direction. Thus, the measurements are in reality more than point measurements and so present a very powerful argument for the existance of isotropy if equation 1-8 is satisfied.

For testing the data equation 1-18 was used which follows directly from equation 1-8. The condition to be satisfied then is $F_v = F_w = 4/3\ F_u$.

Comparison of the results with equation 1-18 over several intervals was made to test for spherical symmetry as an indication of whether or not local isotropy existed. In the periods evaluated spherical (or even axisymmetrical) symmetry was not found. These comparisons are discussed in greater detail in section 4.2 which describes the intervals selected and the results.

4.2 Data Selection and Results

Measurements made on two separate days were chosen for analysis by the technique described in Chapter III. The most appropriate data were obtained on 21 January 1965 and 29 April 1965. From the two recordings selected, 4 12 min periods

of data were analyzed; the interval of 1430-1442* on 29 April 1965, and the intervals of 1220-1232, 1300-1312, and 1308-1320 on 21 January 1965. Calculations of gradient relationships and turbulence characteristics were made and section 4.3 describes the comparison of the two different types of evaluation.

4.2.1 29 April 1965

The general meteorological situation for this day showed most of the nation dominated by an extensive high pressure system centered in northern Texas. It covered the United States except for the northwestern regions. The only other system was a low over the Hudson Bay area in Canada with a front extending through Montana, Idaho, Nevada, and into California. From this front eastward, except for stations along the east coast, almost all stations reported clear skies.

Michigan was under the influence of the high pressure system centered over northern Texas. Willow Run Airport observers reported clear skies except for a few cumulus clouds between 1100 and 1300 hours. Westerly winds prevailed

* All times are Eastern Standard time.

all day with a high of 67°F and a low of 35°F. The relative humidity, after the early morning high, dropped into the mid-twenties and stayed in this region the rest of the daylight hours. The visibility never dropped below 15 miles.

4.2.1.1 Gradient Relationships for the Period of 1430-1442 (4/29/65).

Data obtained from the 4 m tower for 29 April 1965 for 1430-1442 are shown in figure 4-1. The wind data are plotted on the left side and the temperature data on the right. There is a 1.39°C temperature difference between 0.5 and 4 m and the wind profile was very close to logarithmic.

Three combinations of gradient parameters were calculated as a means of relating the turbulence to the mean flow. These were the Richardson number given by

$$Ri = \frac{g\frac{d\theta}{dz}}{\theta(\frac{d\bar{U}}{dz})^2}, \qquad 4\text{-}1$$

the stability factor given by

$$S.F. = \frac{c_p \Delta\bar{\theta}}{\bar{U}^2} \qquad 4\text{-}2$$

and a number closely related to the Richardson number derived by M. A. Wolf (1965) given by

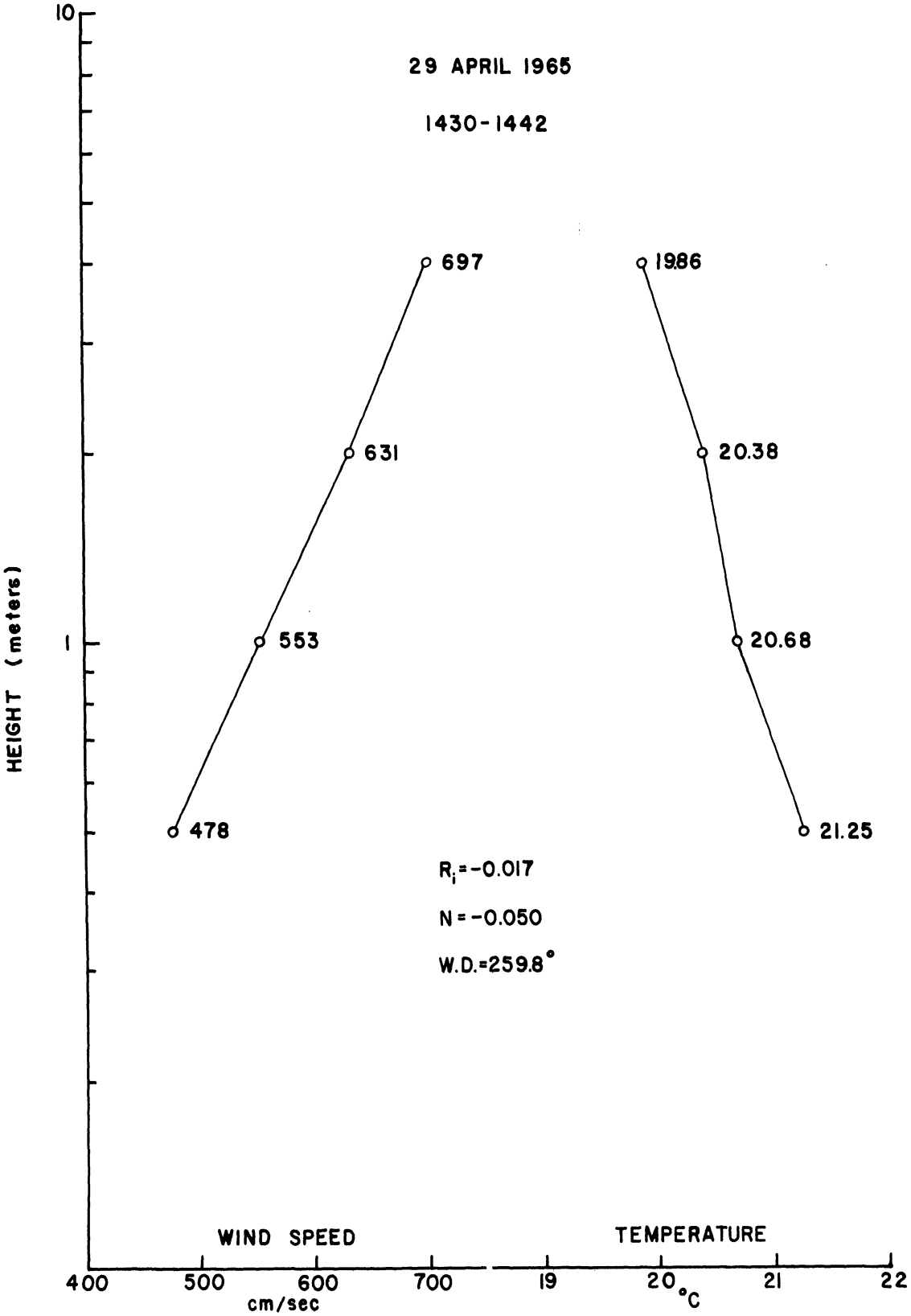

Figure 4-1. Wind and temperature profiles for period 1430-1442 (4/29/65). Measurements were made at 0.5, 1, 2, and 4 m.

$$N = \frac{c_p \frac{d\bar{\theta}}{dz}}{\frac{d\bar{U}^2}{dz}} \qquad 4\text{-}3$$

where g is the gravity, θ is the potential temperature, C_p is the specific heat at constant pressure, T is the absolute temperature, U is the wind speed, and z is the height. For this period $-Ri = 0.017$, $N = -0.050$, and $S.F. = 1.406 \times 10^{-3}$.

N is influenced by both wind speed and wind shear whereas the stability factor and the Richardson number each contain only one of these factors. The Richardson number differs from the stability factor by the term employed in the denominator. While the Richardson number gives an indication of the turbulence initiation, it lacks an indication of the translational energy available for conversion to turbulent energy. The ultimate goal is to be able to relate the turbulent state of the atmosphere to readily measurable quantities as obtained from standard operational instruments. The most widely used technique is to try to relate the turbulence characteristics to the different combinations of the gradients of temperature and velocity. The present study was unable to achieve this goal.

4.2.1.2 Turbulent Characteristics for the Period of 1430-1442 (4/29/65).

Only one 12 min interval was analyzed for 29 April 1965; this was the period from 1430-1442. The spectral densities were computed and multiplied by $U/2\pi$ to convert from a frequency to a wavenumber base. They were then plotted against wavenumber (λ) in logarithmic coordinates. Figure 4-2 shows the results. The straight line is the regression curve obtained by using the least square method applied to the logarithm of both power and wavenumber for the u component of the wind. The resultant regression is

$$W_u = 505\lambda^{-1.71} \qquad 4\text{-}4$$

after the tranformation from a log-log relationship is accomplished. The first two data points as shown in figure 4-2 were not used in the calculations of equation 4-4. The reason for not using these points is discussed below. The correlation coefficient for the regression line in figure 4-2 is $r = -0.9967$.

The slope of -1.71 is in good agreement with the value of -1.67 (or -5/3) expected for the inertial subrange. On the basis of the good agreement between the theory and the observations of the u component of velocity one might infer

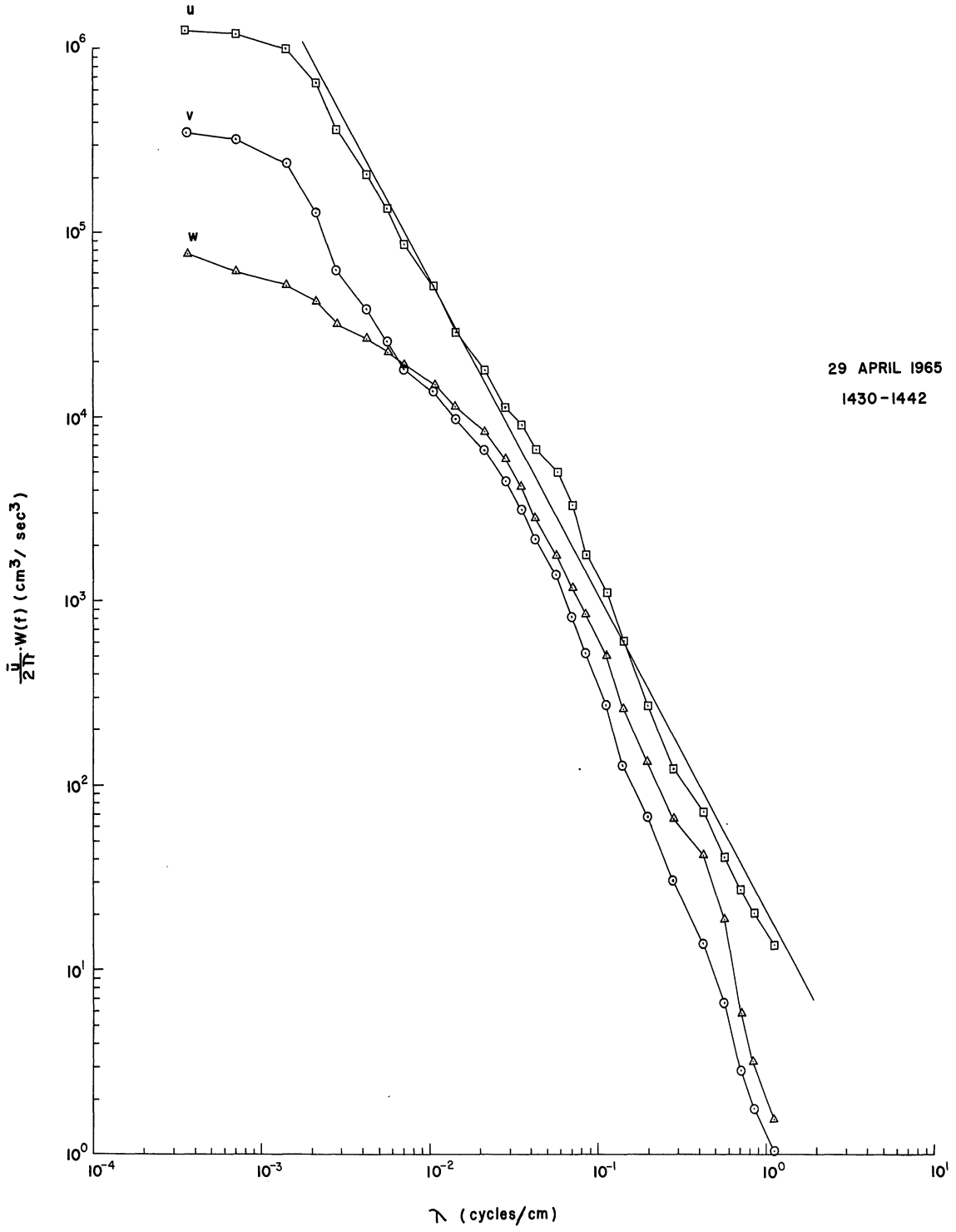

Figure 4-2. Spectral densities for u, v, w for period 1430-1442 (4/29/65) calculated for a bandwidth of 0.3 cps. The straight line is the least square regression line for u (not using the first two data points).

the existance of local isotropy. However, if local isotropy exists, then as pointed out in Chapter I, equation 1-18, the v and w spectral densities should exceed the u spectral density by a factor of 4/3. Examination of figure 4-2 shows no such relationships; in fact, both the v and w spectral densities are <u>less</u> than the longitudinal spectral densities. There is, however, a tendency towards axisymmetrical flow about the x axis (u component) for wavenumbers greater than 7×10^{-3}, except in this region there is an apparent energy input in the w spectrum which shows it to be greater than the v spectrum.

It can be concluded, therefore, that spherical symmetry did not exist during the sampling interval; and, since spherical symmetry is a necessary condition for local isotropy, it can be further concluded that local isotropy did not exist over the sampling interval. Thus, in spite of the excellent agreement between the u spectrum and the theoretical curve, we see that anisotropy exists. Figure 4-2 shows that the inference of local isotropy from an experimental curve of the u component of velocity displaying a -5/3 slope may be incorrect.

Figure 4-3 shows the data plotted in the form of

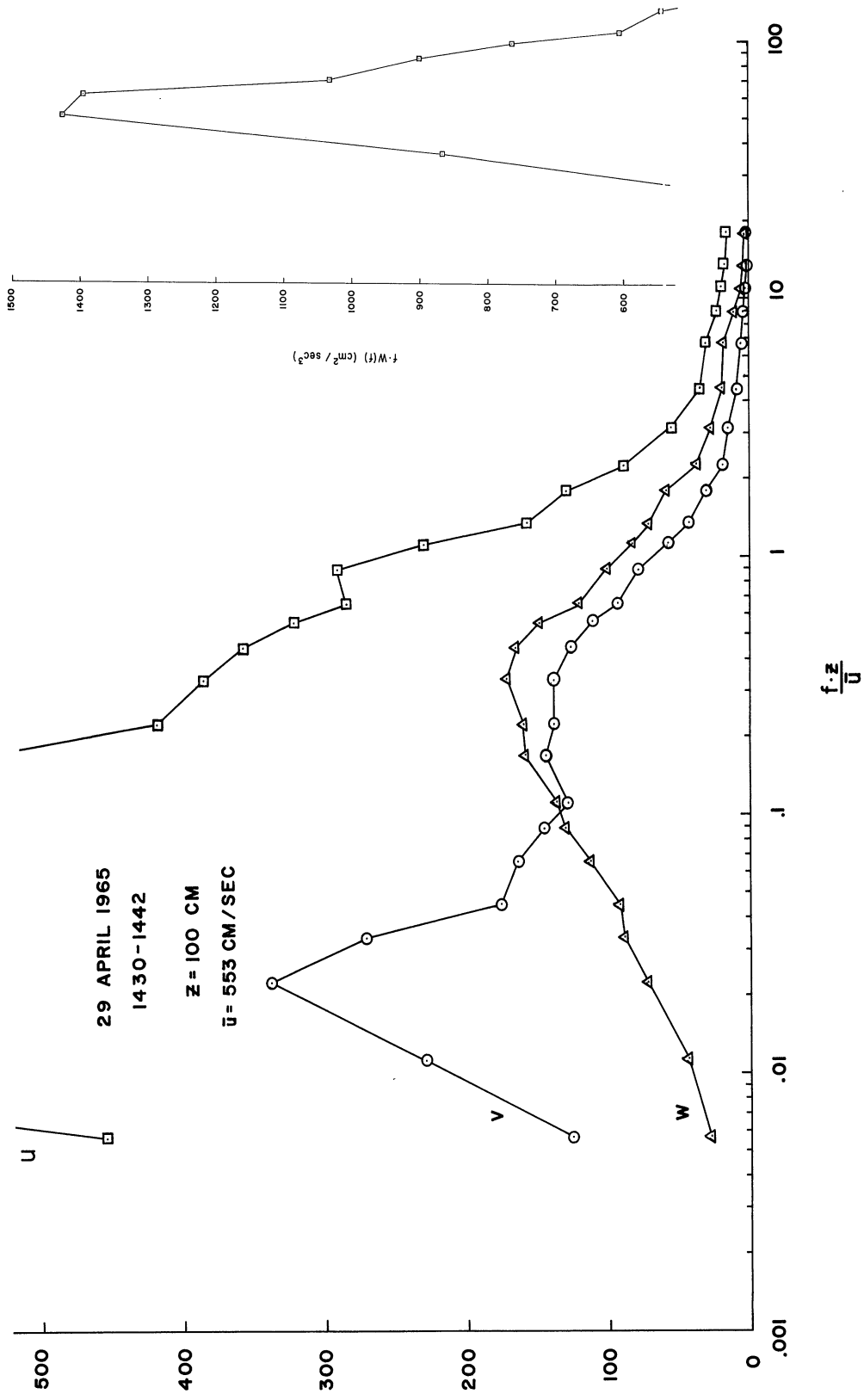

Figure 4-3. Frequency times energy plotted vs. reduced frequency for u, v, w for period 1430-1442 (4/29/65) calculated for a bandwidth of 0.3 cps.

frequency times power versus log reduced frequency. The use of a reduced frequency follows the development of Panofsky and McCormick (1960) in which they show the shape of the vertical (w) spectrum in near neutral or unstable conditions to be independent of stability, roughness, and wind speed. The reduced frequency is achieved by plotting on the abscissa fz/U which allows comparison of spectra at various heights and various wind speeds. Figure 4-3 shows a peak in the w spectrum at a reduced frequency of 0.35, which is in excellent agreement with the results published by Panofsky and McCormick (1960) showing an average of all the peaks to be about 0.2.

The predominant features of figure 4-3 are the peaks of the u and v spectral densities at 0.023. These peaks are seen in all but one of the graphs presented in this study. The only curve that does not display this peak is the w spectrum for 29 April 1965 (figure 4-3). The first question to arise is: "What physical significance can be attached to these peaks?" A characteristic of the peaks is that they all occur at the third data points. This observation leads one to believe that perhaps this peak is not a characteristic of the turbulent regime, but instead a characteristic of the

method of analysis. A detailed analysis of the method of computing the spectrum is given by Portman et.al. (in press) so only the essential points relevent to this low frequency peak will be presented here.

The lower limit of the harmonic wave analyzer used for analysis was 1 cps. It had a bandwidth of 10 cps. Since the data tapes were speeded up for playback from the tape loop by a factor of 32, there was an actual bandwidth for the data of 0.3 cps and a lower frequency limit of 0.03 cps. Thus, the first datum point represents the energy in the bandwidth from 0 to 0.153 cps, while the second point represents the energy in the bandwidth from 0 to 0.156 cps. One would not expect any great difference in the energy as measured by these first two or three points. Looking at figure 4-2 (and indeed figures 4-6, 4-9, and 4-12) one sees a small difference in energy for these first few points. Multiplying by the frequencies (as done in figures 4-3, 4-7, 4-10 and 4-13) which for these first few points were 0.03, 0.06, 0.125, etc., then the first point would be about half of the second point, and the second about half of the third. However, after the first few points, the bandwidth ceases to be the controlling factor and the turbulence

characteristics dominate the rest of the graph. For the above reasons, one should be careful about attaching a physical significance related to the turbulence on the basis of the low frequency peaks of figures 4-3, 4-7, 4-10, and 4-13. For the same reasons, the first two points were not included in the calculation of the least squares regression line given in this chapter.

One expects the maximum wavelength in the vertical spectrum to be about half the height of the measurement. Larger eddies would be "ground up" by the physical barrier of the earth's surface. This does not mean to say that larger eddies are not measured, because it is easy to conceive of the sensing element seeing only the lower portion of a much larger eddy as it passes with its center at some height much above the sensor. The measurements show, therefore, a spectrum of eddies. By converting the peak in the w spectrum of figure 4-3 to a wavelength, and associating this with an eddy size, one obtains the value of 47 cm. Since the sensing element was located at 100 cm, 47 cm is in excellent agreement with the reasoning which calls for eddies to be roughly half the size of the height of measurement.

The v spectrum of figure 4-3 has a plateau in the same region as the peak in the w spectrum. This indicates an input of energy to the v component from the buoyant energy in the w spectrum. It is difficult to envision an eddy passing through a region of the atmosphere and leaving no indication, or trail, of its passage. We see therefore an input of energy which is clearly visible in the v spectrum and noticable in the u spectrum. This violates the Kolmogoroff hypothesis that in the inertial subrange there is no input of energy, but merely a cascade of energy from larger to smaller wavelengths. This introduces the concept of a buoyant subrange whose characteristic wavelength, for at least the first few hundred meters, appears to be a linear function of height (Panofsky and McCormick, 1960).

The buoyant subrange postulated herein is an energy feeding system since it is the medium for energy transfer between the heat source at the surface and the energy containing eddies in the atmosphere. The energy containing region is considered to be the region of eddies between the equilibrium region and the long permanent waves in the atmosphere. The buoyant subrange is in the high frequency end of the energy containing region.

Panofsky appears reluctant to identify this region as a buoyant subrange (see, for example, Panofsky and McCormick, 1960 and Lumley and Panofsky, 1964, p. 169) because of the strong dependence of the turbulence structure on the mechanical affect of the surface. However, it is felt that, near the surface, the presence of the ground acts as a restraint on the buoyant subrange as well as a source of production. Thus, we envision the buoyant subrange as being caused by convective motions but strongly influenced by the presence of the ground.

At a height of about 200 m the equilibrium range has a limit on the long wave end of 400 to 600 m due to an energy sink suggested by Bolgiano (1962). For a stably stratified atmosphere, he points out that "the equilibrium range will now normally exhibit a new portion, a buoyancy subrange at the lower end of the spectrum, in which gravity effects are significant. The group of parameters on which the structure depends must be enlarged so as to represent the gravity force and the fluctuations in density as well as the rate of dissipation of turbulent kinetic energy. Since in the buoyancy subrange the dissipation rate ϵ is no longer synonymous with the rate of transfer of kinetic energy across the

spectrum, we are led to the further postulate that, in this interval, ϵ may be discarded."

The concepts stated by Bolgiano (1962) show his "buoyancy subrange" to be an energy sink wherein eddies are damped by stable stratification. He also places the "buoyancy subrange" at the low frequency end of the equilibrium range, and included in it. This is incompatible with the equilibrium range as defined in this study wherein the range is considered a conservative system with no energy sinks or sources.

Bolgiano (1962) developed an expression for the spectral functions; however, he started with the basic assumption of axisymmetrical flow about the z axis. He states that "for the most part, in the free atmosphere the lapse of temperature is less than adiabatic and that the medium is, therefore, stably stratified. In spite of this fact there is convincing evidence (Kellogg, 1956) of the existence of random, irregular motion in the free atmosphere at all times. We may conclude that, with the exception of very limited, intensely stable strata, the atmosphere is simultaneously turbulent and stably stratified." Since the temperature gradient is one-dimensional in the z direction and turbulence

is three-dimensional, for a stable atmosphere the interaction of the two would directly damp only the vertical structure of turbulence, and only indirectly affect the horizontal structure. Thus the assumption of axisymmetry about z is not unreasonable. Figure 4-3 indicates, however, that if there is any tendency towards axisymmetrical flow for this period, it is about the x axis and not the z axis as one might expect.

Because of the existance of the buoyant subrange (not the Bolgiano buoyancy subrange) in the wavelengths where one expects to find the inertial subrange and because local isotropy is not indicated by the data anywhere in the range of measurements, it is concluded that there is an insufficient bandwidth between the buoyant energy input and the ultimate dissipation for an equilibrium region to establish itself. There is strong evidence of the existance of the equilibrium region at greater heights in the atmosphere (MacCready, 1962, Shur, 1962 and Reiter and Burns, 1966) so there must be some height above the surface where the bandwidth between energy input and dissipation becomes wide enough for an equilibrium region to be established. One would expect the height where local isotropy begins to be a function of the existing

atmospheric conditions. The data collected during this study were insufficient to form an estimate of the height where one might expect to find an equilibrium region. The low wavelength limit of the data presented in this study is of the order of a centimeter. Hinze (1959, p. 7) states that "for moderate flow velocities, that is, not much greater than, say, 100 m/sec, the smallest space scale or eddy will hardly be less than about 1 mm ...", which is only one order of magnitude smaller than the lower wavelength considered in the present study. One would not expect, therefore, that this bandwidth would be sufficient for any significant change in the turbulence structure. Figure 4-4 presents a schematic representation of the various spectral regions as a function of height.

The efforts to relate the turbulence structure as shown in figure 4-2 and figure 4-3 to the gradient relationships will be discussed after the rest of the data are presented.

4.2.2 21 January 1965

The general meteorological situation for 21 January 1965 showed most of the nation under the influence of a double high pressure system with one well-developed high

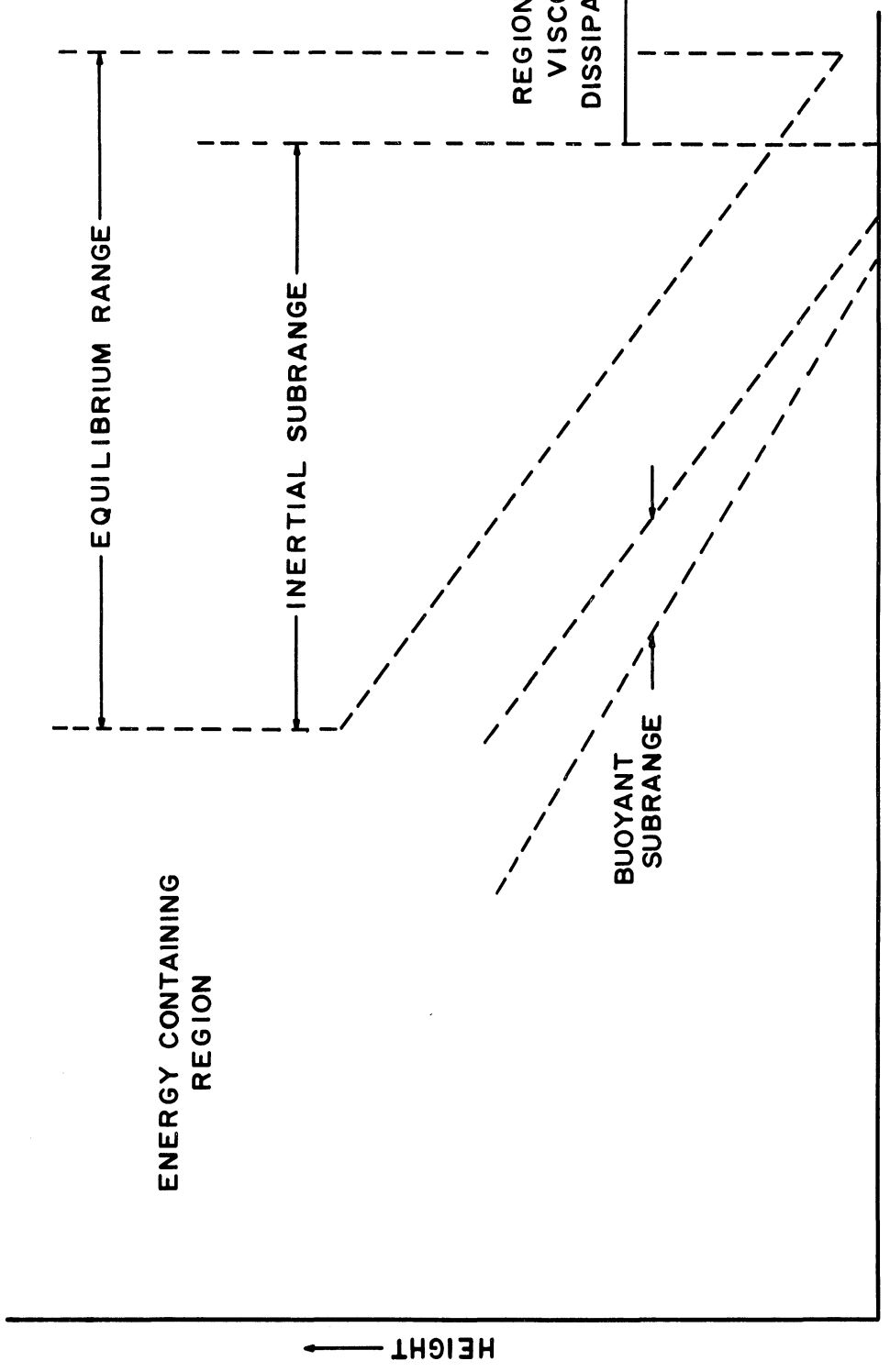

Figure 4-4. Schematic representation of the various spectral regions as a function of height based on the results of others and the analysis as presented in this study.

centered over southern Indiana and northern Kentucky, and another weaker high center over Idaho. These highs were separated by a weak trough extending from a low north of Winnipeg through Bismarck, Rapid City, Denver, and into a low just southwest of El Paso. Another low pressure system located over the mouth of the St. Lawrence River had a front extending southeast into the Atlantic and then curving back west, entering the United States south of Norfolk, Va., extending through North Carolina, northern Georgia, Alabama and through central Mississippi.

Michigan was under the influence of the high pressure centered over southern Indiana and except for the period between 1100 and 1300 hours Willow Run had a clear sky. The temperature during the period was about 24°F with about a two-degree rise per hour. There were about one-tenth coverage of stratocumulus clouds at 1600 feet and at 1247 there was just a trace of snow. The ground at the field site had a snow depth of one inch and the maximum temperature for the day was 29°F with a minimum of 9°F.

Three periods were analyzed on this day and they are presented as the three 12-minute intervals of 1220-1232, 1300-1312, and 1308-1320.

4.2.2.1 Gradient Relationships for the Period of 1220-1232 (1/21/65).

The wind profile and temperature profile are presented in figure 4-5. The temperature lapse from 0.5 to 4 m was 0.61°C. The Richardson number of -0.018 is very nearly the same as the number for 29 April. The wind direction was 220° N, which includes the affects of wind speed, was -0.032. The stability factor was 6.38×10^{-3}.

4.2.2.2 Turbulent Characteristics for the Period 1220-1232 (1/21/65).

The spectral densities for this period are shown in figure 4-6 plotted vs. wavenumber (λ). The least square regression line for the u component is given by

$$W_u = 595\lambda^{-1.93}. \qquad 4\text{-}5$$

The correlation is given as r = -0.9842. Inspection of figure 4-6 shows that the u spectrum is bow-shaped and could possibly be broken into two regions. The low frequency (except the first two points) shows a fairly straight region out to $\lambda = 6 \times 10^{-2}$ and another more steeply sloped region from this point to the high frequency end of the graph. The bow-shaped feature of the u spectrum is seen to exist in varying degrees in the graphs presented in this form

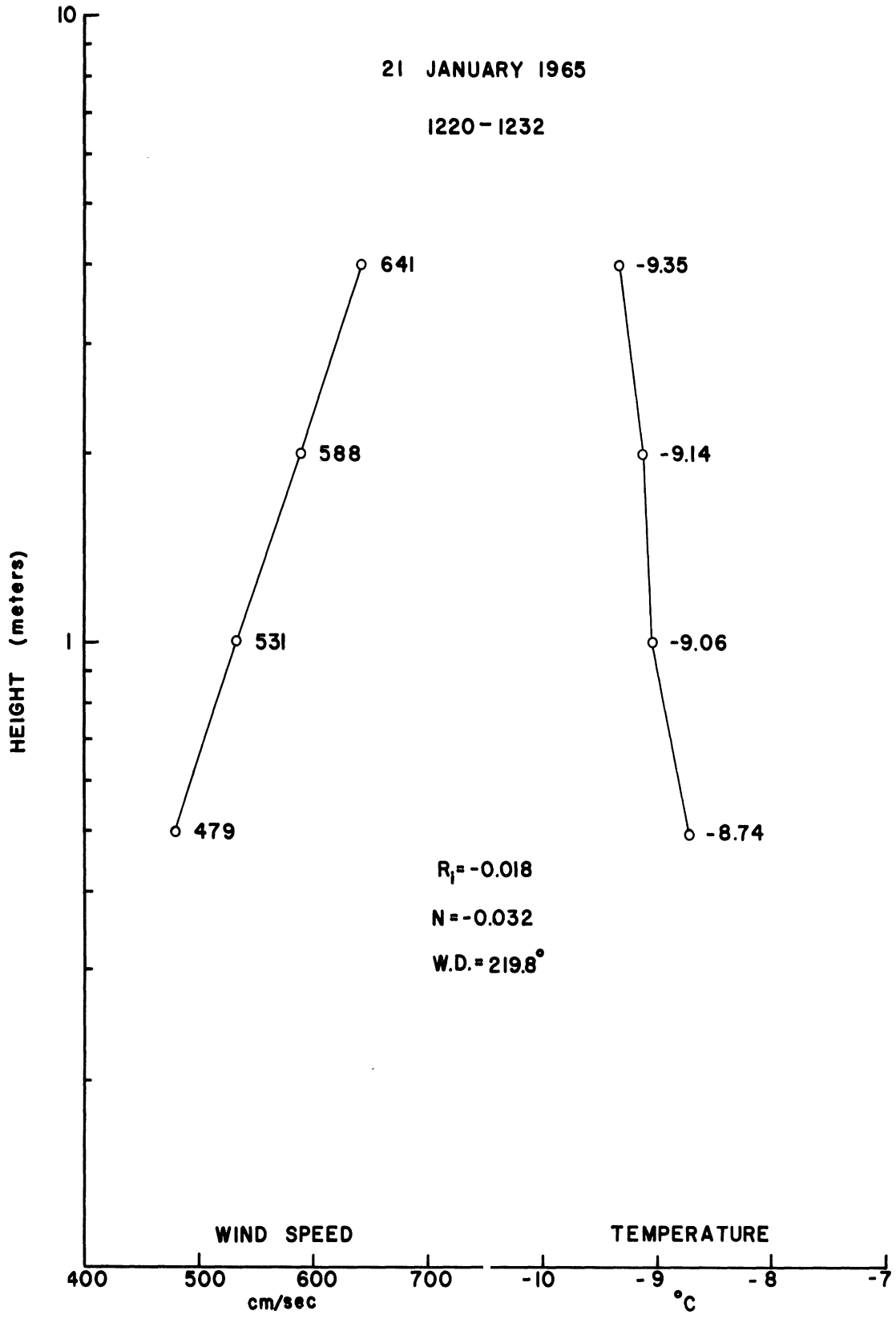

Figure 4-5. Wind and temperature profiles for period 1220-1232 (1/21/65). Measurements were made at 0.5, 1, 2, and 4 m.

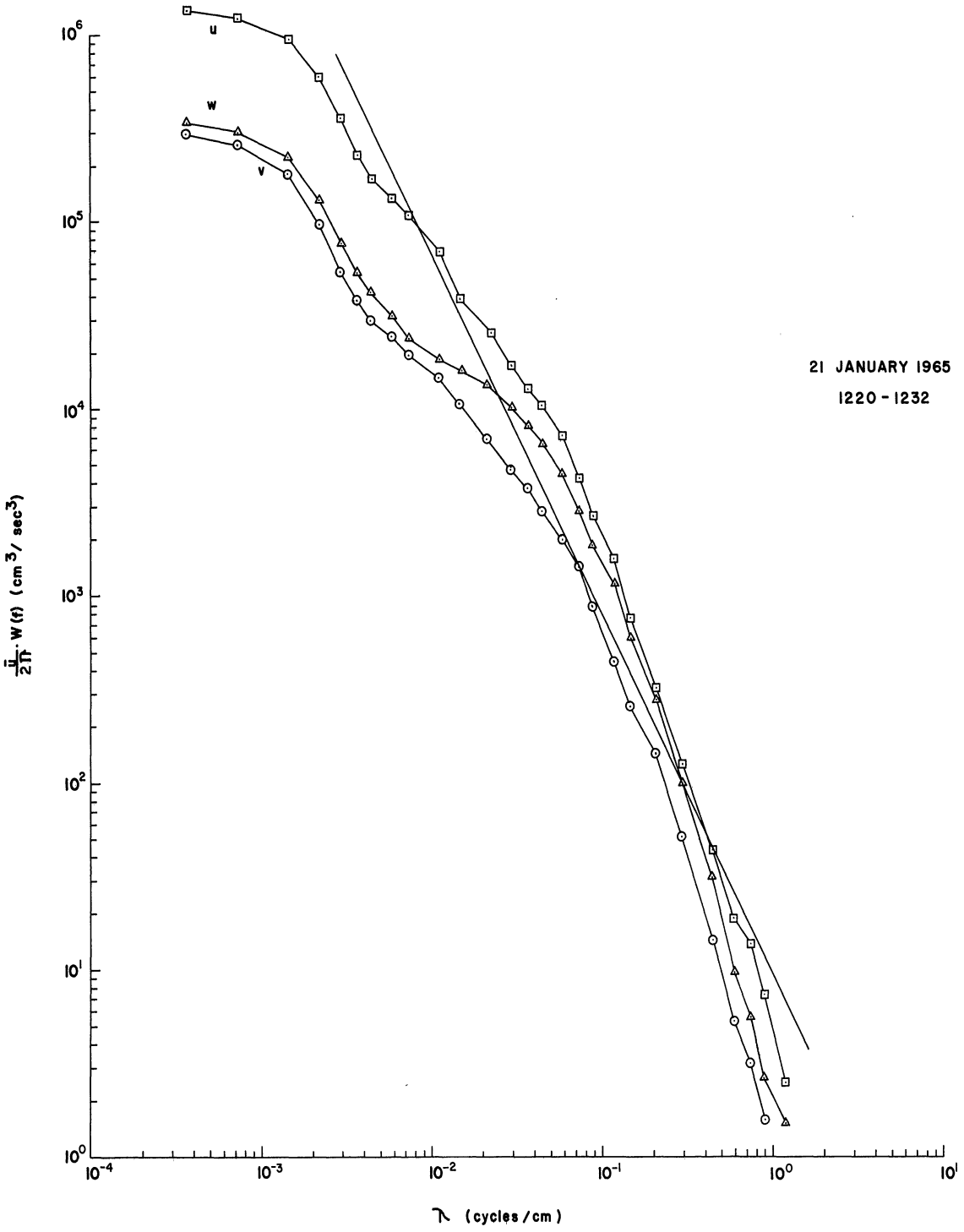

Figure 4-6. Spectral densities for u, v, w for period 1220-1232 (1/21/65) calculated for a bandwidth of 0.3 cps. The straight line is the least square regression line for u (not using the first two data points).

(figures 4-2. 4-6, 4-9, and 4-12). The bow shape is least developed in figure 4-2 for 29 April 1965 and the best developed for this period (1220-1232, 1/21/65). In all the graphs this "breaking point" between the two slopes occurs very close to the peaks in the w spectrum as seen in figures 4-3, 4-7, 4-10, and 4-13, so that the input of energy in this region is due to buoyancy affects.

An eddy size associated with the peak in the w spectrum of figure 4-7 works out to be 34 cm with the peak at a reduced frequency of 0.5. This result is in good agreement with the expected value for the wavelength, and the peak is in good agreement with the value of 0.2 obtained from Panofsky and McCormick (1960). Figure 4-7 shows that the v spectrum is not as strongly influenced by the buoyancy affects as was that presented in figure 4-3 (1430-1442, 4/29/65). The broad peak in the v spectrum is not as close to the w peak as was the v and w spectrum for the April 29 period. This indicates a smaller transfer of energy from the buoyancy into eddy components in the lateral direction. It is difficult to conceive how the presence of buoyant eddies could avoid influencing the u spectrum. In a very crude example, we can imagine an eddy moving

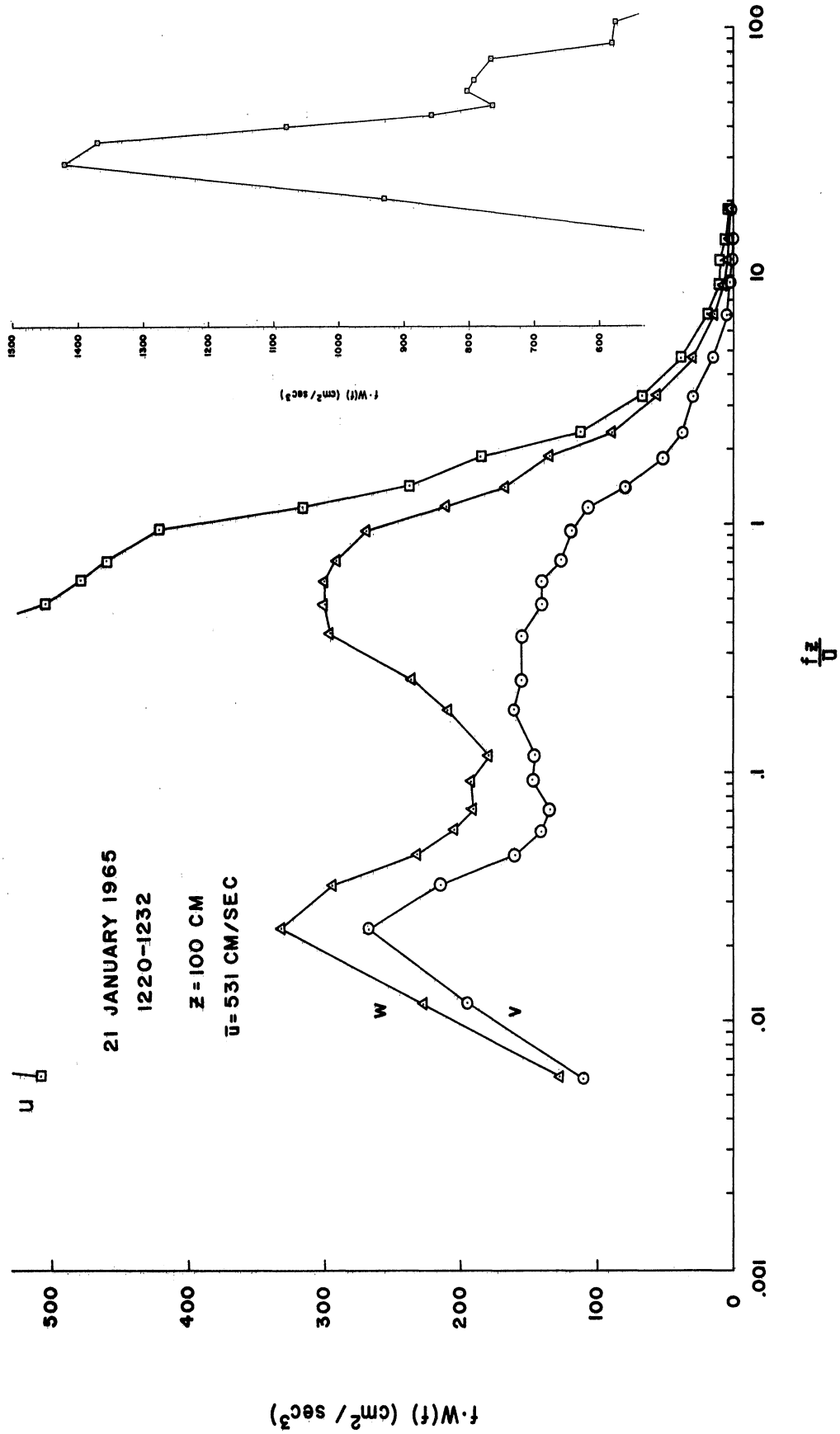

Figure 4-7. Frequency times energy plotted vs. reduced frequency for u, v, w for period 1220-1232 (1/21/65) calculated for a bandwidth of 0.3 cps.

upward through a turbulent medium under the influence of buoyancy forces. Since the eddy is coming from surroundings of less momentum, it would now exert a drag on its new surroundings by viscous forces. This would tend to increase the energy in this particular wavelength, which is seen in the u spectrum as measured in this study.

4.2.2.3 Gradient Relationships for the Period 1300-1312 (1/21/65).

Figure 4-8 presents the mean flow measurements for this period. The temperature lapse between 0.5 and 4 m is 0.63°C and the Richardson number is -0.019, N = -0.032, and S.F. = 5.91×10^{-3}. The average wind direction over the interval is 212°.

4.2.2.4 Turbulent Characteristics for the Period 1300-1312 (1/21/65).

The regression curve for the u spectrum for this period is

$$W_u = 374\lambda^{-1.92} \qquad 4\text{-}6$$

which shows (as was found for the period of 1200-1232) a slope greater than the -5/3 expected. This indicates a deficiency in the cascade of energy to higher frequencies

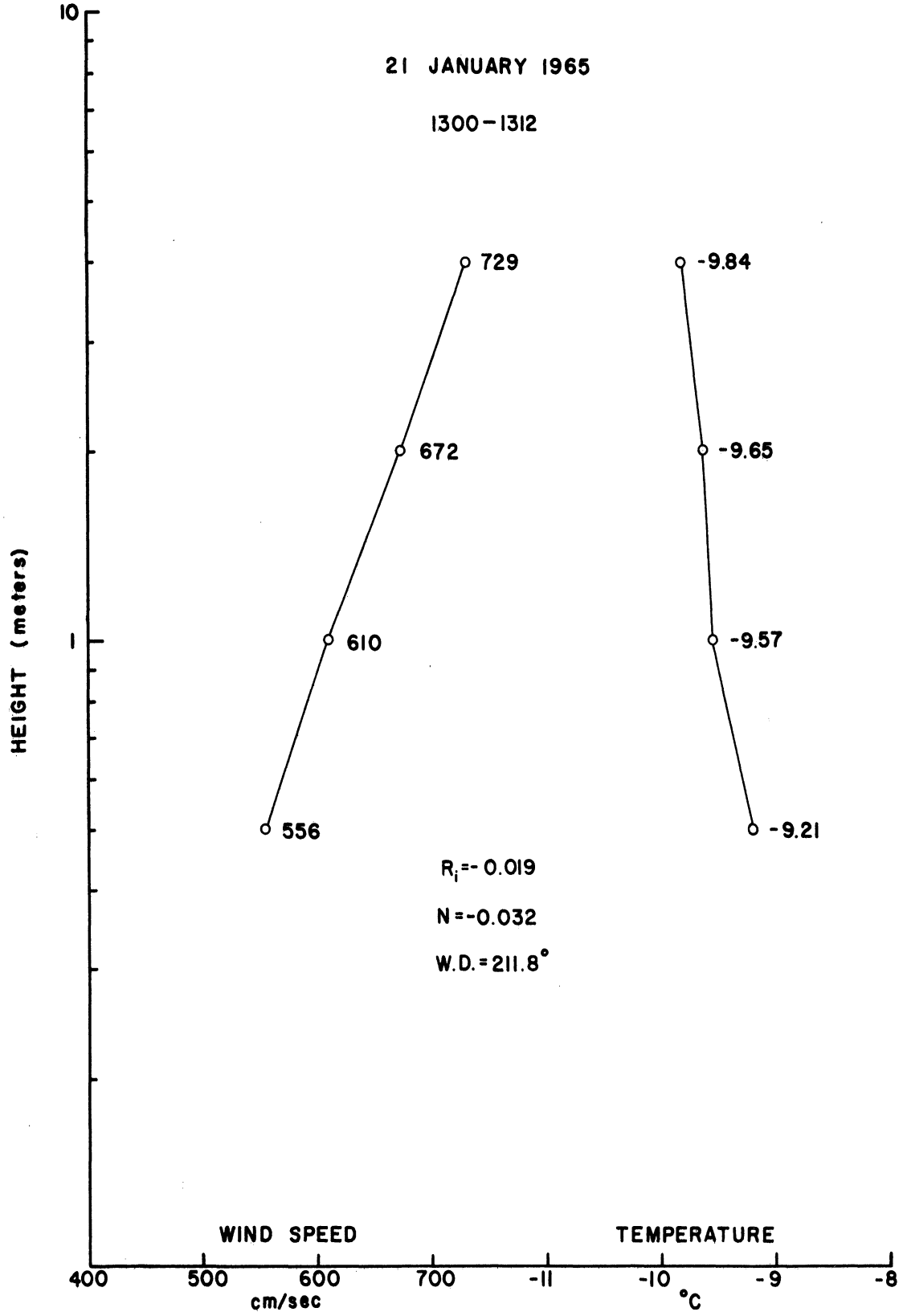

Figure 4-8. Wind and temperature profiles for period 1300-1312 (1/21/65). Measurements were made at 0.5, 1, 2, and 4 m.

so that the observed values are less than predicted by the theory.

A very interesting feature of figure 4-9 is that in the interval $3 \times 10^{-2} < \lambda < 5.7 \times 10^{-1}$ the spectrum of w shows more energy than the longitudinal component. From isotropic considerations, one might think that this represents a tendency towards isotropy. However, the same tendency is not observed in the v component, indicating that the energy in the w spectrum is a buoyant affect rather than a cascade of energy. This result is illustrated again in figure 4-10 which shows the peak of the buoyant energy input at $\lambda = 3.5 \times 10^{-2}$ or a reduced frequency of 0.54. This peak value corresponds to an eddy wavelength of 29 cm.

Figure 4-10 shows a definite influence on the u spectrum near the buoyant subrange with a peak at a reduced frequency of 0.33. There is a small peak in the v spectrum at 0.165 which is believed to be due to the influence of the buoyancy effects. However, there is even less buoyancy effects noticable in the v spectrum than is seen in the previous period (1220-1232, 1/21/65). The most pronounced affect is in the u spectrum which shows a marked input of energy at the higher frequencies associated with the buoyant subrange.

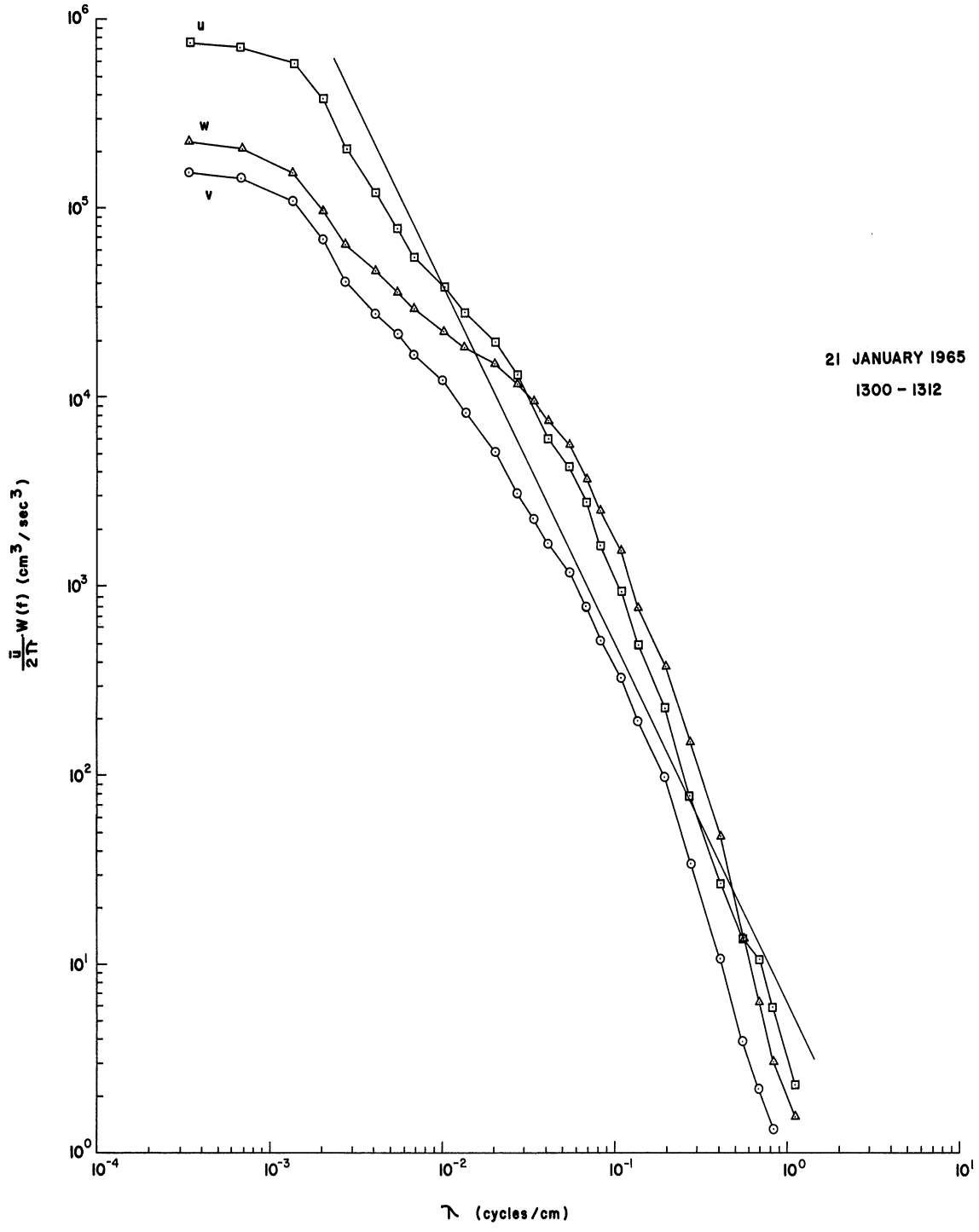

Figure 4-9. Spectral densities for u, v, w for period 1300-1312 (1/21/65) calculated for a bandwidth of 0.3 cps. The straight line is the least square regression line for u (not using the first two data points).

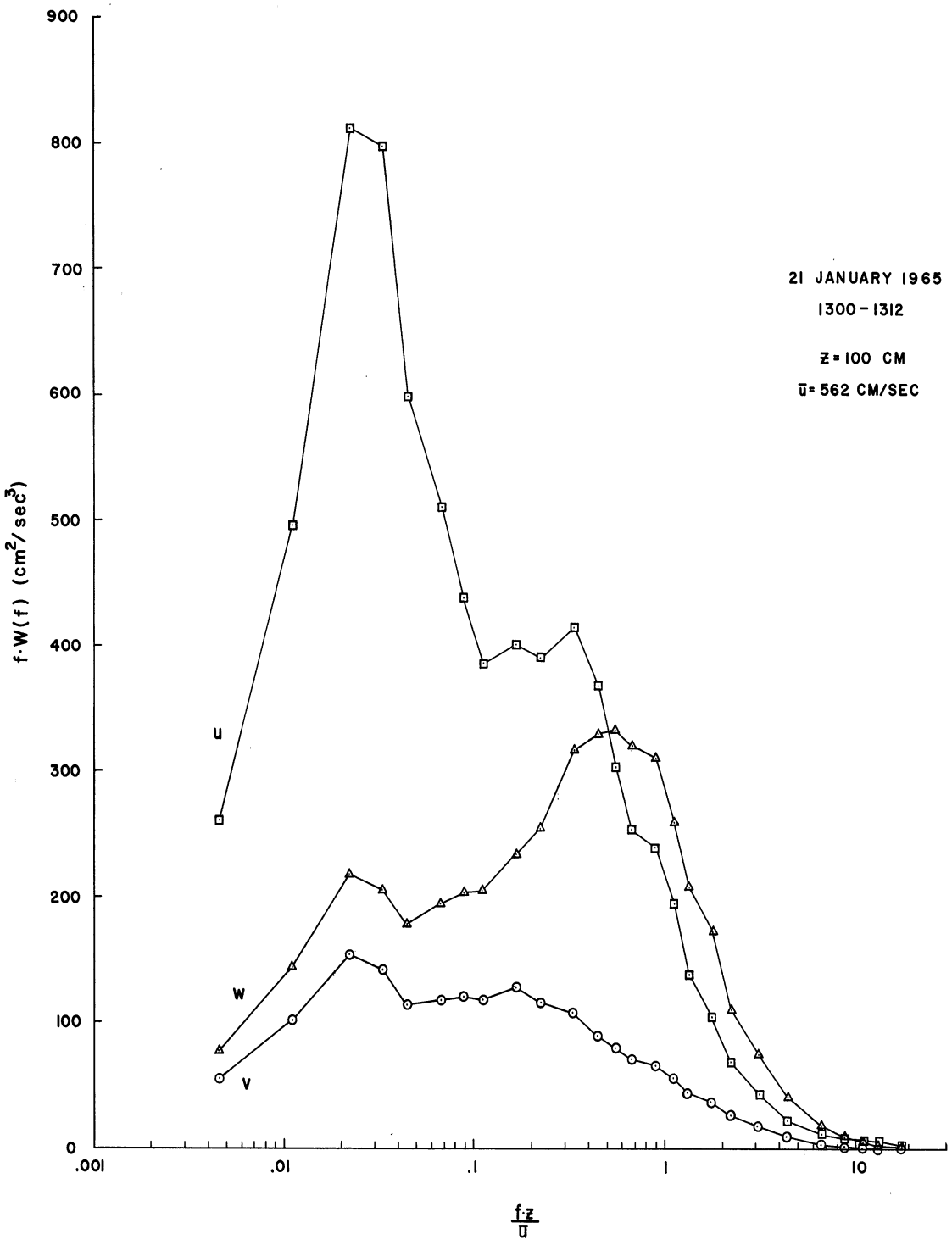

Figure 4-10. Frequency times energy plotted vs. reduced frequency for u, v, w for period 1300-1312 (1/21/65) calculated for a bandwidth of 0.3 cps.

4.2.2.5 Gradient Relationships for the Period of 1308-1320 (1/21/65).*

The mean flow measurements for this period are given in figure 4-11. The temperature lapse between 0.5 and 4 m is 0.72°C. The Richardson number equals -0.015, S.F = 5.51×10^{-3}, and N = -0.028. The average wind direction for the interval is 214°.

4.2.2.6 Turbulent Characteristics for the Period 1308-1320 (1/21/65).

The regression equation for the longitudinal component for this period is given by

$$W_u = 388\lambda^{-1.78} \qquad 4\text{-}7$$

with a correlation coefficient r = -0.9886. Again we see (figure 4-12) the affects of buoyancy in that the w spectrum

* This period overlaps by 4 min the previous period (1300-1312, 1/21/65) because of several physical problems associated with the data reduction equipment. One reel of digital tape holds only 20 min of data, and the digital programs were written to accommodate only one data tape at a time. The analog loop recorder could hold 105 ft of analog tape and at the record speed used was able to record 12 min of data at a time. In order to break the 20 min digital tape into two 12 min intervals required then this 4 min overlap.

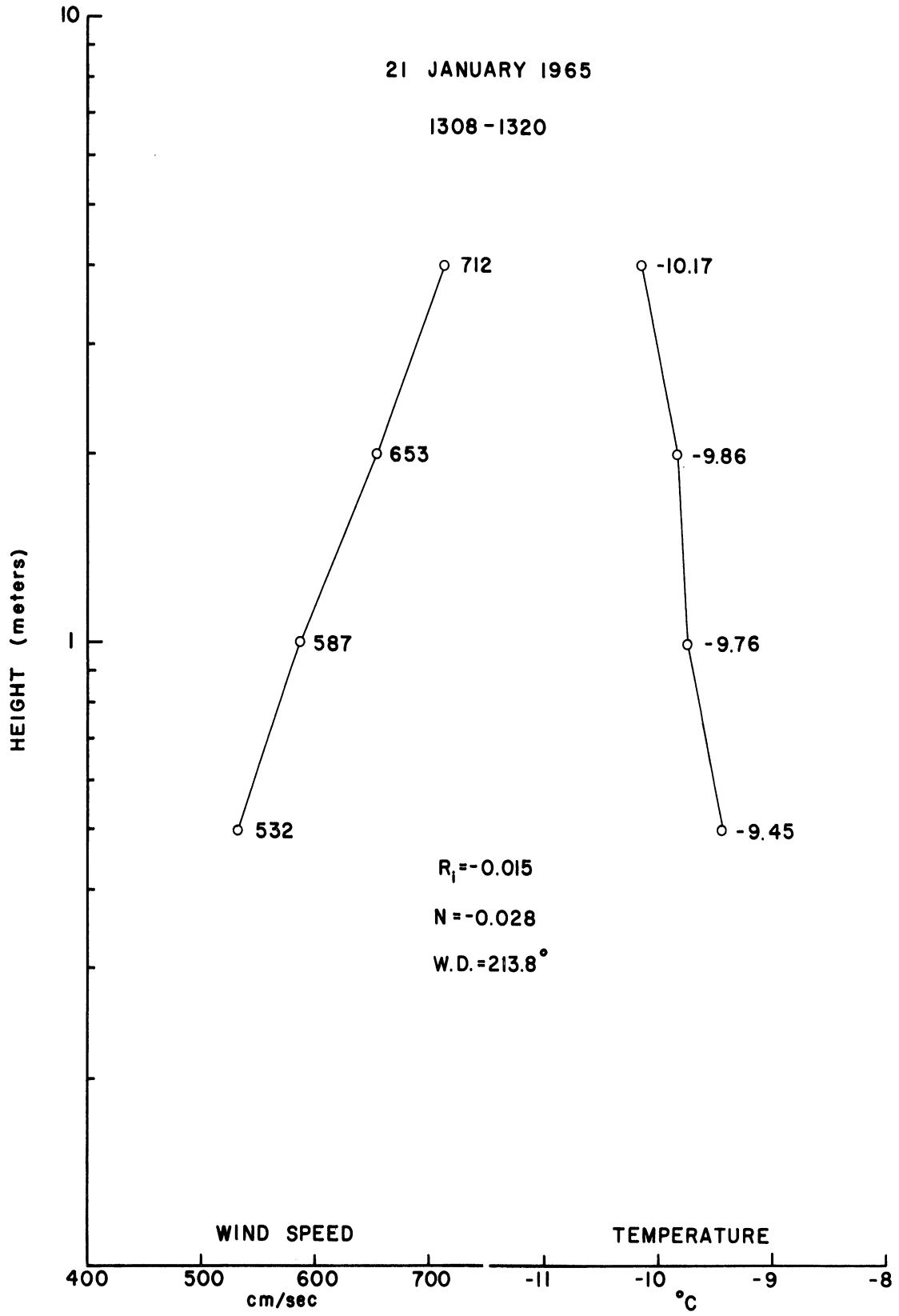

Figure 4-11. Wind and temperature profiles for period 1308-1320 (1/21/65). Measurements were made at 0.5, 1, 2, and 4 m.

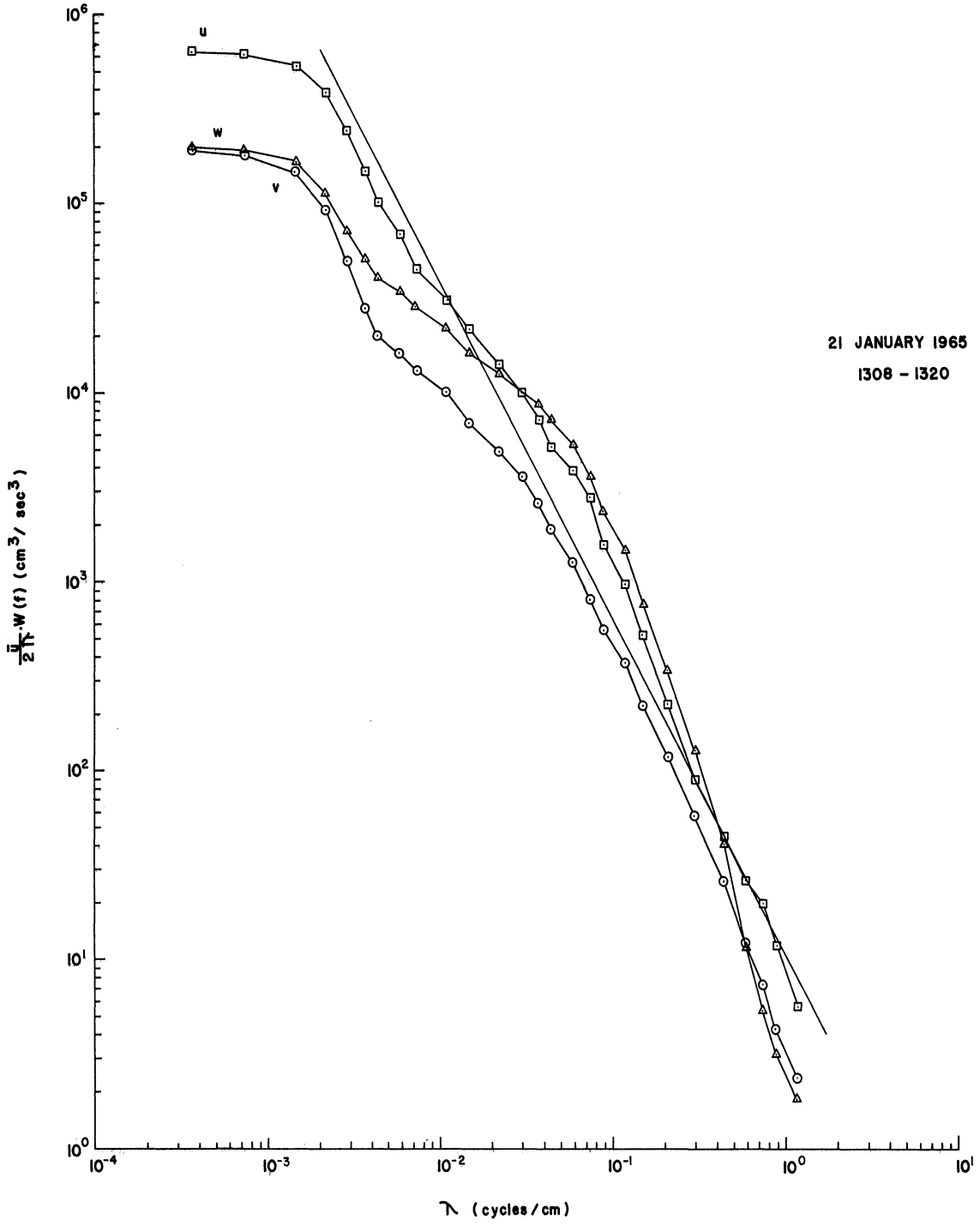

Figure 4-12. Spectral densities for u, v, w for period 1308-1320 (1/21/65) calculated for a bandwidth of 0.3 cps. The straight line is the least square regression line for u (not using the first two data points).

exceeds the u spectrum between the wavenumbers $3 \times 10^{-2} < \lambda < 4 \times 10^{-1}$. The energy input shows a marked influence in the u spectrum (figure 4-13) but much less influence on the v spectrum. This period (1308-1320, 1/21/65) shows a very marked decrease in the w spectrum at the high frequency relative to the v spectrum. For $\lambda > 5.6 \times 10^{-1}$ (figure 4-12) the w spectrum is less than the v spectrum, which is the only occurrence of this at the high frequencies in the four periods analyzed. The first period (1430-1442, 4/29/65) showed the w spectrum in the low frequencies to be less than the v spectrum; however, at frequencies above the region of the buoyant subrange, the v spectrum was the smaller of the two.

Figure 4-13 shows the buoyant subrange to peak at a reduced frequency of about 0.6 to 0.7. This corresponds to an eddy size of about 25 cm.

4.3 Comparison of Turbulence and Gradient Relationships

In addition to the parameters already given, an estimate of the surface roughness, z_o, was made by extrapolating the wind profile to the height of zero wind speed. For 29 April 1965 when the ground had a 3 cm grass cover,

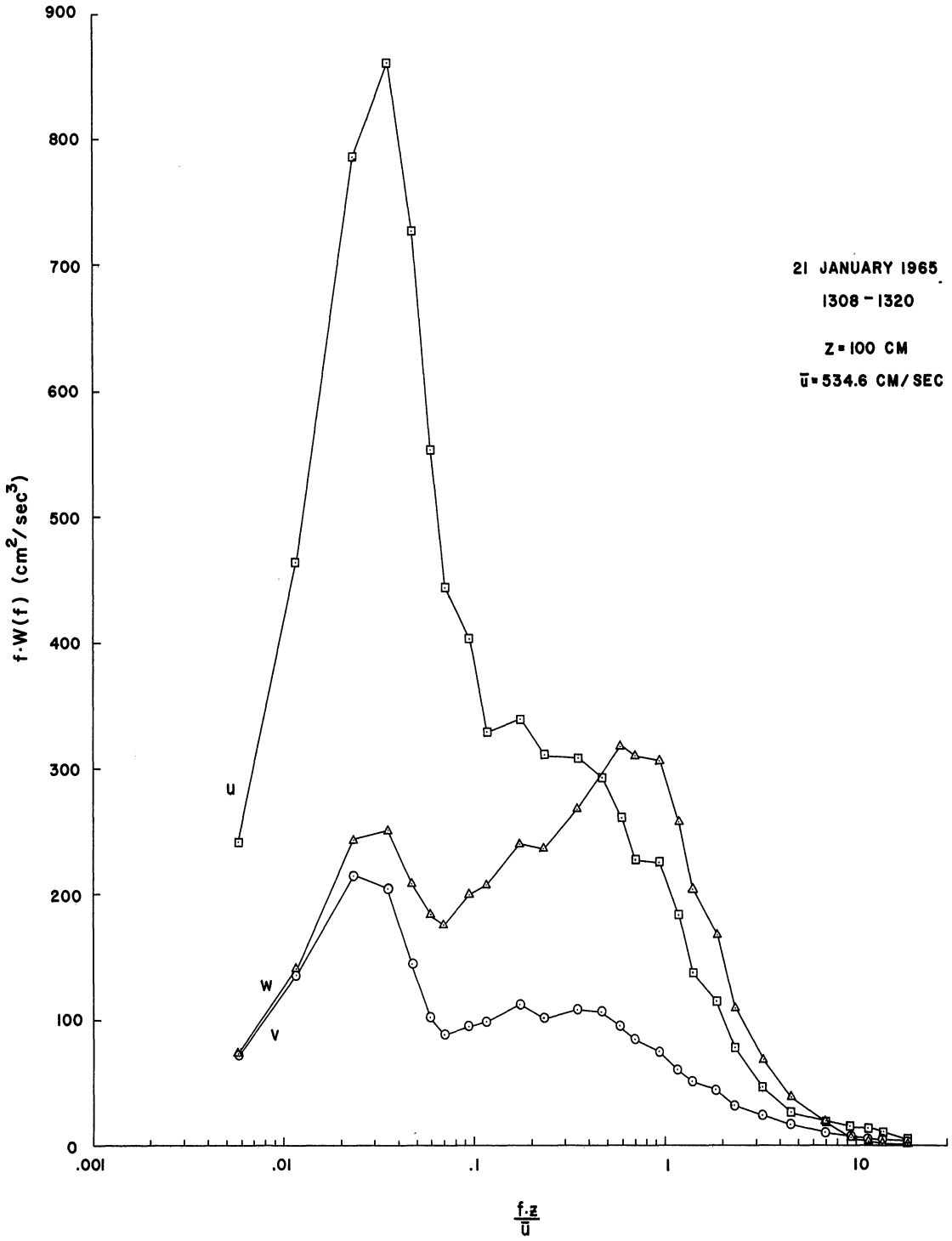

Figure 4-13. Frequency times energy plotted vs. reduced frequency for u, v, w for period 1308-1320 (1/21/65) calculated for a bandwidth of 0.3 cps.

the surface roughness parameter was 0.64 cm. On 21 January 1965 with a 1 in snow cover, the z_o parameters for the three profiles of 1220-1232, 1300-1312, and 1308-1320 were computed to be 0.11, 0.10, and 0.10 cm respectively. Table 4-1 gives a summary of the parameters calculated by the various gradient techniques. In addition to the gradient relationships, several characteristics of the turbulent regime are listed as deduced from the values used to plot the spectral graphs.

There are essentially three quantities that should affect the turbulent regime: 1) the velocity field, 2) the temperature field, and 3) the surface roughness. The velocity field contains two combinations of parameters: 1) the wind speed which when squared gives an indication of the translational energy available for conversion to turbulent energy, and 2) the variation of wind speed with height which is an indication of the shear affects in a layer.

The temperature field usually is defined in a vertical sense so that variations of temperature with height give an indication of buoyant effects.

Since all the hot wire measurements described herein were taken at 100 cm above the surface, the surface roughness

Table 4-1

Gradient and Turbulence Parameters for the Selected Intervals.

Gradient Relationships

	4/29/65	1/21/65		
	1430-1442	1220-1232	1300-1312	1308-1320
$Ri_{100\ cm}$	-0.017	-0.018	-0.019	-0.015
$N_{100\ cm}$	-0.050	-0.032	-0.032	-0.028
Temperature Lapse (50-400 cm)	-1.39	-0.61	-0.63	-0.72
Wind $Speed_{100\ cm}$	553	531	610	587
Stability $Factor_{100cm}$ ($\times 10^5$)	1406	.638	591	551
z_o	0.64	0.11	0.10	0.10

Turbulence Parameters

Slope of Regression Curve for u	-1.71	-1.93	-1.92	-1.78
A (in Regression Equation)	505	595	374	338
Correlation for u	-0.9967	-0.9842	-0.9842	-0.9886
Buoyant Peak (λ)	0.0213	0.0296	0.0349	0.0367
Buoyant Peak (W·f)	174	300	333	317
Low Frequency Peak (W·f)	1427	1419	814	860
Buoyant Peak (Wavelength)	47	34	29	25

has to be considered as an important factor for inducing mechanical turbulence.

Combinations of the wind and temperature fields are given by the Richardson numbers, stability factors, and N numbers shown in Table 4-1 as defined early in this chapter (equations 4-1, 4-2, and 4-3). The Richardson number shows very little variation among the four intervals, so that as a discriminator for the turbulent regime it is of no value.

N is able to distinguish between the two separate days; however, on the basis of N one would conclude that the 29 April 1965 results would show stronger buoyant effects than the three periods of 21 January 1965. Looking at the amplitude of the peaks in the buoyant subrange we see that on 29 April 1965 the amplitude was 174 cm/sec^2 while the 21 January 1965 day showed amplitudes of 300, 333, and 317 cm/sec^2 for the three periods. So that even though N is able to show the two days as different, it is in the wrong sense. N, however, is fairly closely related to the wavelength of the eddy associated with the buoyant peak in the w spectrum. Whether this is significant or merely a coincidence is not too clear. Many more comparisons would need to be made before a definite statement could be made about a relationship between N and

this particular eddy scale.

Looking at the u spectra we see that the 29 April 1965 period and the period of 1220-1232 (1/21/65) had rather large values as shown by the low frequency peak, while the other two period (1300-1312 and 1308-1320) had much lower peaks. The same result is seen in the calculation of A in the least squares regression. This difference between the first two and last two periods is not reflected in any of the gradient relationships.

By arguing that a decrease in surface roughness would decrease the transfer of energy from larger to smaller wavelengths (or from lower to higher frequencies) one would expect a steeper slope on the 21 January 1965 periods since the surface roughness was a factor of six smaller for these periods than on the 29 April 1965 period. Table 4-1 shows that a steeper slope is observed for the three periods in January indicating an absence of the mechanical turbulence needed to feed the higher frequencies.

The last two periods (1300-1312 and 1308-1320) as represented in figures 4-10 and 4-13 show the w spectral energy to be greater than the u spectral energy in the higher frequencies. This is due to the combination of a lack of

energy available at the lower frequencies and a deficiency of transfer to the higher frequencies because of a smaller surface roughness.

4.4 Summary

A technique has been developed for extending the measurement of the structure of atmospheric turbulence to smaller scales than has previously been possible. Recent advances in the state of the art of hot wire anemometry for the constant temperature mode of operation has permitted the adaptation of this instrument for use in atmospheric studies. By proper alignment of several wires, the three components u, v, and w of the wind were obtained and spectral relationships computed. The data were recorded on an analog magnetic tape recorder and later reduced by using both analog and digital computational techniques.

The sensing element of the hot wire anemometer was located at a height of 1 m above the ground. Temperature lapse conditions occurred during the four time periods analyzed. Mean flow data were available from three cup anemometers and vertical temperature gradients from shielded thermocouples, all mounted on a 4 m tower. The study

involved the analysis of mean flow and gradient properties as well as the turbulent fluctuation statistics. No definite relationships appeared between the gradient parameters and the measured turbulence properties. However, a connection was found between the surface roughness and the slope of the u spectrum suggesting that, near the surface, z_o is an important parameter affecting the transfer of energy from lower to higher frequencies.

The analysis reveals a buoyant subrange at frequencies beyond the sensing capability of most meteorological equipment. Such an input of buoyant energy demonstrates, for the conditions studied, that Kolmogoroff's hypothesis of local isotropy cannot exist at these frequencies and, if the equilibrium range is to be found, it must be at even higher frequencies. The high frequency limit of the measurements extends to wavelengths of the order of one centimeter; it is believed that the smallest possible discrete eddy must be no more than one millimeter. It is difficult to conceive that the statistical properties of the turbulence reach equilibrium within this narrow range of wavelengths.

The peak of the buoyant subrange occurs at frequencies agreeing with those obtained in earlier studies which show

a linear dependence with height above the ground. The bandwidth between the buoyant subrange and the range of viscous dissipation increases with height. At some height the bandwidth becomes large enough to permit the establishment of the equilibrium range. From the data collected in this study the height at which equilibrium is first established can not be determined. The analysis supports the hypothesis that the upper limit of local isotropy is a linear function of height near the surface. It does not support, however, the idea that the upper limit is given by twice the height above the ground.

Appendix*

METEOROLOGY COMPUTING LABORATORY

Department of Meteorology and Oceanography
The University of Michigan, Ann Arbor

The Meteorology Computing Laboratory, consisting of analog and digital computers was established under National Science Foundation Grant GP-805 during 1963 and 1964. Some parts of the system, the digital computer, became operational during the summer of 1963. The system was virtually complete by spring of 1964 and has been extensively utilized ever since.

1. Description of the Meteorology Computing Laboratory

The Meteorology Computing Laboratory comprises two computer systems, one analog and one digital, and a linkage system. This logical segmentation is equally applicable to the modes of use of the computing equipment. Each computer system can be used individually or they may be used jointly. The linkage system cannot be used without involving both the analog and the digital computer systems.

A. The Digital Computer System

The digital computer system is based on the Control Data Corporation 160-A computer with the following peripheral

* This Appendix is an abridged version of an unpublished report describing the Meteorology Computing Laboratory by Fred V. Brock.

equipment: two magnetic tape units, a digital plotter, an on-line typewriter and a high speed paper tape punch and reader.

(1) CDC 160-A Computer. The 160-A computer is a parallel, binary machine with a core storage of 8192 12 bit words. The memory cycle time is 6.4 μ sec. Two input/output channels are provided one of which is buffered to permit simultaneous input/output or input/output while computing. A priority interrupt is provided to facilitate external timing control.

(2) Digital Plotter. The plotter, a CALCOMP Model 565, enables direct digital plotting. This plotter moves in fixed increments of 0.01 inch at the maximum rate of 300 increments per second.

(3) On-line Typewriter. The on-line typewriter is used for low-volume input/output such as messages to the operator and commands from the operator.

(4) Paper Tape Reader and Punch. Paper tape is used as a source program medium as well as for data input. The reader will accept any format paper tape at a rate up to 350 characters per second. The punch operates at 110 characters per second.

(5) Magnetic Tape Units. Two magnetic tape units are provided which use IBM compatible tape format at low density (200 bits per inch). Tape speed is 75 inches per second which gives a transfer rate of 15000 characters per second. These units are used for storage of library programs, data storage, data input, and communication with the IBM 7090 in the University Computing Center.

(6) Programming Aids. The principal programming aids, provided by Control Data Corporation, are an assembler, OSAS-A, and a FORTRAN II type compiler, 160-A FORTRAN. Fortran has been augmented to include analog input/output and to permit control of the linkage system. Many other programming packages are provided by Control Data and the 160-A users group SWAP but OSAS and FORTRAN are used almost exclusively.

B. Analog Computer System

The analog computer system comprises three Applied Dynamics Model AD-2-64 PBC analog computers, two X-Y plotters, an 8 channel strip chart recorder, and an oscilloscope display.

(1) Analog Computers. The three analog computers may be used as independent computers with complete control

features including digital volt meters or they may be slaved together to operate as one large computer. The three computers have about the same complement of computing elements and each is equipped to operate either in real time or in repetitive mode. The total complement of computing elements is given in the following table.

Analog Computer Equipment

Amplifiers		136
Integrator/Summers	72	
Summers	24	
Inverters	40	
Coefficient Potentiometers		330
Multipliers, Electronic		36
Function Generators (Sine, Cosine, Square, Log., Variable)		24
Comparators		9
Function Switches		33
Digital Volt Meters		3

(2) Analog Output Devices. Two 11 by 17 inch X-Y plotters and an 8-channel strip chart recorder are available for recording analog outputs. An X-Y oscilloscope is used

for observing output when operating in the repetitive mode. The oscilloscope display can be photographically recorded via a standard oscilloscope camera or a specially adapted movie camera.

C. Linkage System

The linkage system provides communication and control between the analog and digital computers. Five modes of communication or control are possible: analog to digital, digital to analog, digital output from the 160-A, digital input to the 160-A, and interrupt control of the 160-A.

(1) Analog to Digital. Analog input to the 160-A is provided via a low speed multiplexer, a high speed multiplexer and a converter. There are 16 analog inputs. The low speed multiplexer selects one of two groups of 8, one group for the $\pm$ 100 volt range and the other for the $\pm$ 10 volt range. The high speed multiplexer presents one of the eight in sequential order to the converter to be translated into an equivalent digital signal. The conversion rate at present is 10,000 conversions per second. The converter uses the full 12 bit word which provides a resolution of 5 millivolts or 50 millivolts depending on whether the 10 or the 100 volt range is used.

(2) Digital to Analog. Analog output from the 160-A is provided via a digital memory and 8 digital to analog converters. When the 160-A outputs a word to the linkage system it is held in the memory and presented to one of the converters which produces an analog voltage which is held until up-dated by the 160-A. The output range is $\pm$ 10 volts. This range can be adjusted as desired in the analog computer by setting the appropriate input gain to an amplifier.

(3) Digital Output. Digital output from the 160-A is decoded, one word at a time, in the linkage system to enable control of the analog computers. The mode (POT SET, INITIAL CONDITION, OPERATE, HOLD) of each analog computer can be set and a repetitive operation cycle can be initiated. To facilitate reading the output of various analog components the digital output can select any amplifier, integrator summing junction, coefficient potentiometer or trunk line to be presented to the analog to digital coverter. In addition digital output can be used to operate 12 relays in the analog computers, select analog input voltage range, and enable external interrupts.

(4) Digital Input. Twelve digital values comprising one 12 bit word can be read by the 160-A to detect external

conditions such as whether a relay is open or closed.

(5) Interrupt. There are two interrupt lines which can be used to signal external events to the 160-A. For example an accurate timing source may be used to generate an interrupt to control analog to digital conversion.

BIBLIOGRAPHY

Batchelor, G. K., 1947: Kolmogoroff's theory of locally isotropic turbulence. Proc. Camb. Phil. Soc., 43, 533-559.

_____, 1960: The theory of homogeneous turbulence. Cambridge University Press, 197 pp.

Blackadar, A. K., H. A. Panofsky, S. Berman, J. K. S. Ching, G. D. Hess, J. E. Oliphant, 1965: Flux of heat and momentum in the planetary boundary layer of the atmosphere. Final Report No. 8604, The Pennsylvania State University.

Blackman, R. B. and J. W. Tukey, 1958: The measurement of power spectra. Dover Publications, Inc., 190 pp.

Bolgiano, R., Jr., 1962: Structure of turbulence in stratified media. J. Geophys. Res., 67, No. 8, 3015-3024.

Bradshaw, P., and R. F. Johnson, 1963: Turbulence measurements with hot wire anemometers. National Physical Laboratory Notes on Applied Science No. 33, Her Majesty's Stationery Office, London.

Brock, F. V., 1965: Meteorology computing laboratory, Department of Meteorology and Oceanography, The University of Michigan, Ann Arbor. (Unpublished report.)

_____, and D. J. Provine, 1962: A standard deviation computer. J. App. Met., 1, No. 1, 81-90.

Cramer, H., 1955: The elements of probability theory. John Wiley and Sons, Inc., 281 pp.

Dryden, H. L., 1943: A review of the statistical theory of turbulence. Q. App. Math., 1, 7-42.

Eschenroeder, A. Q., 1965: A turbulence spectrum for shear flows. Technical Report TR65-11B, General Motors Corporation, GM Defense Research Laboratories, Santa Barbara, California.

BIBLIOGRAPHY (continued)

Fano, R. M., 1950: Short-time autocorrelation functions and power spectra. J. Acoust. Soc. Amer., 22, 546-550.

Flow Corporation Bulletin No. 68, 1962: X-wire turbulence measurements. Cambridge, Massachusetts.

Flow Corporation Bulletin No. 47B, 1963: Flow corporation hot wire probes. Cambridge, Massachusetts.

Flow Corporation Bulletin No. 94, 1964: Hot wire measurements of air velocity and direction. Cambridge, Massachusetts.

Gifford, F., 1956: The relation between space and time correlations in the atmosphere. J. Met., 13, 289.

Hinze, J. O., 1959: Turbulence. McGraw-Hill Book Company, Inc., 586 pp.

Hoel, P. G., 1954: Introduction to mathematical statistics. John Wiley and Sons, Inc., 331 pp.

Holloway, J. L., Jr., 1958: Smoothing and filtering of time series and space fields. Advances in Geophys., 4, Academic Press, Inc. 351-391.

Holmes, R. M., and H. W. Carson, 1964: Carbon dioxide flux in nature. Plant Research Institute, Canada Department of Agriculture. (Unpublished report.)

Jenkins, G. M., 1963: An example of the estimation of a linear open loop transfer function. Technometrics, 5, No. 2, 227-245.

Kellogg, W. W., 1956: Diffusion of smoke in the stratosphere. J. Met., 13, 241-250.

BIBLIOGRAPHY (continued)

King, L. V., 1914: On the convection of heat from small cylinders in a stream of fluid. Phil. Trans. Roy. Soc. 214, 373.

Kolmogoroff, A. N., 1941: The local structure of turbulence in incompressible viscous fluid for very large Reynolds numbers. Comptes rendus (Doklady) de l'Academie des sciences de l'U.R.S.S., 30, 301-305.

_____, 1941: On degeneration of isotropic turbulence in an incompressible viscous liquid. Comptes rendus (Doklady) de l'Academie des sciences de l'U.R.S.S., 31, 538-540.

_____, 1941: Dissipation of energy in locally isotropic turbulence. Comptes rendus (Doklady) de l'Academie des sciences de l'U.R.S.S., 32, 16-18.

Kovasznay, L. S. G., 1943: Calibration and measurement in turbulence research by the hot wire method. NACA Techn. Memorandum No. 1130.

_____, L. T. Miller and B. R. Vasudeva, 1963: A simple hot wire anemometer. Project Squid Tech. Report JHU-22-P. The Johns Hopkins University.

Kraichnan, R. H., 1963: Approximations for steady-state isotropic turbulence. Research Report No. 3, Contract Nonr. 3999(00), Peterborough, New Hampshire.

_____, 1963: Decay of isotropic turbulence in the direct-interaction approximation. Research Report No. 4, Contract Nonr. 3999(00), Peterborough, New Hampshire.

Lappe, U. O., and B. Davidson, 1963: On the range of validity of Taylor's hypothesis and the Kolmogoroff spectral law. J. At. Sciences, 20, No. 6, 569-576.

BIBLIOGRAPHY (continued)

Lettau, H. H., 1963: Studies of the effect of variations in boundary conditions on the atmospheric boundary layer. Annual Report, University of Wisconsin.

Lin, C. C., 1948: Note on the law of decay of isotropic turbulence. Proc. Nat. Ac. Sci., 34, 540-543.

_____, 1953: Taylor's hypothesis and the acceleration terms in the Navier-Stokes equations. Q. Appl. Math., 10, 295-306.

_____, 1961: Statistical theories of turbulence. Princeton University Press, 60 pp.

Lumley, J. L., and S. Corrsin: A random walk with both Lagrangian and Eulerian statistics. Printed by Spottiswoode, Ballantyne and Co., Ltd., London and Colchester.

_____, and H. A. Panofsky, 1964: The structure of atmospheric turbulence. Interscience Publishers, 239 pp.

MacCready, P. B., Jr., 1962: Turbulence measurements by sailplane. J. Geophy. Res., 67, No. 3, 1041-1050.

_____, 1962: The inertial subrange of atmospheric turbulence. J. Geophy. Res., 67, No. 3, 1051-1060.

_____, 1964: Mean wind speed measurements in turbulence. Paper presented at the National Conference on Micrometeorology, Salt Lake City, Utah, Oct. 13-15, 1965.

Miyake, M., 1961: Transformation of atmospheric boundary layer induced by inhomogeneous surfaces (Growth of internal boundary layer). Master's Thesis, University of Washington.

_____, 1965: A constant temperature wind component meter development and application. University of Washington, Final Report AT(45-1)-1545.

BIBLIOGRAPHY (continued)

Obukhov, A. M., 1962: Some specific features of atmospheric turbulence. J. Geophy. Res., 67, No. 8, 3011-3014.

Ogura, Y., 1953: The relation between the space- and time-correlation function in a turbulent flow. J. Met. Soc. Japan, 31, 355.

Otterman, Joseph, 1960: The properties and methods for computation of exponentially-mapped-past statistical variables. IRE Transactions on Automatic Control, AC-5, No. 1, 11-17.

Panofsky, H. A., and R. A. McCormick, 1960: The spectrum of vertical velocity near the surface. Q. J. R. M. Soc., 86, No. 370, 495-503.

Pasquill, F., 1962: Atmospheric diffusion. D. Van Norstrand Company, Ltd., 297 pp.

Payne, F. R., 1964: Airborne investigation of atmospheric turbulence. Master's Thesis, The Pennsylvania State University.

Pond, S., R. W. Stewart, and R. W. Burling, 1963: Turbulence spectra in the wind over waves. J. Atmos. Sciences, 20, No. 4, 319-324.

_____, 1965: Turbulence spectra in the atmospheric boundary layer over the sea. pt. 1 and 2. Manuscript Report No. 19. Institute of Oceanography, The University of British Columbia.

Portman, D. J., F. C. Elder and E. Ryznar, 1961: Research on energy exchange processes. Pubn. No.7 , Great Lakes Res. Div., Inst. Sci. and Techn., University of Michigan

_____, F. C. Elder, E. Ryznar and V. E. Noble, 1962: Some optical properties of turbulence in stratified flow near the ground. J. Geophy. Res., 67, No. 8, 3223-3235.

BIBLIOGRAPHY (continued)

Portman, D. J., E. Ryznar, A. A. Waqif, (in press): Laser scintillation caused by turbulence near the ground. Cold Regions Research and Engineering Laboratory Research Report.

Prandtl, L., 1925: Bericht uber Untersuchungen zur ausgebildeten Turbulenz. Z. angew. Math. Mech., 5, 136-139.

_____, 1927: Ueber die ausgebildete Turbulenz. Verh. 2. int. Kongr. techn. Mechanik, Zurich, 1926, pp. 62-74.

Priestley, C. H. B., 1959: Turbulent transfer in the lower atmosphere. The University of Chicago Press, 130 pp.

Reiter, E. R., and A. Burns, 1966: The structure of clear-air turbulence derived from "TOPCAT" aircraft measurements. J. Atmos. Sci., 23, No. 2, 206-212.

Reynolds, Osborne, 1894: On the dynamical theory of incompressible viscous fluids and the determination of the criterion. Proc. roy. Soc. Lond., 56, 40-45 (Abstr.).

Rouse, H., 1963: On the role of eddies in fluid motion. Am. Sci., 51, No. 3, 285-314.

Ryznar, E., 1965: Dependency of optical scintillation frequency on wind speed. App. Opt., 4, No. 11, 1416-1418.

Sandborn, V. A., 1959: An equation for the mean velocity distribution of boundary layers. NASA Memorandum M-2-5-59E.

_____, and R. D. Marshall, 1965: Local isotropy in wind tunnel turbulence. Colorado State University, Report CER 65VAS-RDM71.

BIBLIOGRAPHY (continued)

Schubauer, G. B., and C. M. Tchen, 1961: Turbulent flow. Princeton University Press, 123 pp.

Shur, G. N., 1962: Experimental investigations of the energy spectrum of atmospheric turbulence. Aerospace Information Division, Report T-63-55.

Singer, I. A., M. E. Smith, and E. W. Bierly, Editors, 1965: Conference on AEC meteorological activities, May 19-22, 1964. Brookhaven National Laboratory BNL 914(C-42).

Sutton, O. G., 1953: Micrometeorology. McGraw-Hill Book Company, Inc., 333 pp.

Tatarski, V. I., 1961: Wave propagation in a turbulent medium. McGraw-Hill Book Company, Inc., 285 pp.

Taylor, G. I., 1921: Diffusion by continuous movements. Proceedings of the London Mathematical Society, Ser. 2, 20, 196-211.

_____, 1932: The transport of vorticity and heat through fluids in turbulent motion. Proc. of the Royal Society, Series A., 135, 685-701.

_____, 1935: Statistical theory of turbulence, Parts I-IV. Proceedings of the Royal Society, Ser. A, 151, 421-478.

_____, 1938: The spectrum of turbulence. Proceedings of the Royal Society, Ser. A., 164, 476-490.

Tieleman, H. W., and V. A. Sandborn, 1965: A three-dimensional single roughness element in a turbulent boundary layer. Colorado State University, Report CSU-9-T-SPC.3.

Townsend, A. A., 1956: The structure of turbulent shear flow. Cambridge University Press, 315 pp.

Uberoi M. S., and S. Corrsin, 1953: Diffusion of heat from a line source in isotropic turbulence. NACA Report No. 1142.

BIBLIOGRAPHY (concluded)

von Karman, T., 1924: Uber die Stabilitat der Laminar-stromung und die Theorie der Turbulenz, Proc. 1st Inter. Congr. Appl. Mech., Delft, p. 97.

_____, 1948: Progress in the statistical theory of turbulence. J. Mar. Res., 7, 252-264.

_____, and L. Howarth, 1938: On the statistical theory of isotropic turbulence. Proc. of the Roy. Soc., Ser. A, 164, 192-215.

Walker, E. R., 1965: Micrometeorological measurements of wind components and temperature variability at Suffield, Alberta. Suffield Special Publication 53, Defense Research Board, Dept. of National Defense, Canada.

Wolf M. A., 1965: Turbulence criteria derived from conventional atmospheric measurements. Technical Memorandum No. PMR-TM-65-1, Pacific Missile Range, Point Mugu, California.

UNIVERSITY OF MICHIGAN
3 9015 02229 0913